THE ASTROPHYSICAL JOURNAL SUPPLEMENT SERIES, 128:213–243, 2000 May

A THREE-POSITION SPECTRAL LINE SURVEY OF SAGITTARIUS B2 BETWEEN 218 AND 263 GHz. II. DATA ANALYSIS

A. NUMMELIN,[1] P. BERGMAN, AND Å. HJALMARSON
Onsala Space Observatory, SE-439 92 Onsala, Sweden; nummea@rpi.edu, bergman@oso.chalmers.se, hjalmar@oso.chalmers.se

P. FRIBERG
Joint Astronomy Center, 660 North A'ohoku Place, University Park, Hilo, HI 96720; friberg@jach.hawaii.edu

W. M. IRVINE
FCRAO, 619 Lederle GRC, University of Massachusetts, Amherst, MA 01003; irvine@fcrao1.phast.umass.edu

T. J. MILLAR
Department of Physics, UMIST, P.O. Box 88, Manchester M60 1QD, UK; tjm@saturn.phy.umist.ac.uk

M. OHISHI
Research Center for Development of Far-Infrared Region, Fukui University, 3-9-1 Bunkyo, Fukui 910-8507, Japan; saito@maxwell.apphy.fukui-u.ac.jp

AND

S. SAITO
Institute for Molecular Science, Myodaiji, Okazaki 444, Japan; saito@ims.ac.jp
Received 1999 June 21; accepted 1999 November 10

ABSTRACT

We present an analysis of the data from our Swedish-ESO Submillimetre Telescope molecular line survey in the 1.3 mm band of the N, M, and NW positions in the Sgr B2 molecular cloud. The line emissions from 42 molecular species, and some of their isotopomers, were analyzed assuming a single temperature and a homogeneous source. In cases where a source size much smaller than the antenna beam (23″) could be estimated, optical depth effects were also accounted for. In this way rotation temperatures, molecular column densities, and in several cases also source sizes, were determined. Observed and modeled intensities are presented in rotation diagrams. A few complex molecular species, NH_2CHO, CH_3CHO, C_2H_3CN, C_2H_5CN, and CH_3OCHO, mainly in the N source, exhibit anomalously strong intensities in their intrinsically weak *b*- and *c*-type lines. We argue that this effect can hardly be explained by high optical depths alone, and therefore propose that the possibility of radiative pumping via the low-lying vibrational states of these molecules should be investigated as an alternative explanation. The highest rotation temperatures, up to about 500 K, were found for large molecules toward Sgr B2(N), closely followed by Sgr B2(M). In Sgr B2(NW), which samples the cloud envelope, the rotation temperatures are 15–50 K. For molecules with too few observed transitions to allow determination of rotation temperatures, the column density was calculated assuming optically thin emission, and we adopted rotation temperatures of 50, 50, and 20 K in M, N, and NW, respectively. Column density ratios of isotopomers were determined. After a critical discussion of the resolution-dependent H_2 column density toward the observed positions, abundances relative to H_2 were calculated. We discuss the chemical differences between the three observed cloud positions and compare with the hot core, compact ridge, and outflow in Orion A. Hot core-type molecules like CH_2NH, NH_2CN, CH_3CN, C_2H_3CN, and C_2H_5CN, as well as H_2CS, are more abundant in Sgr B2(N) by factors of 3–8 as compared to the M position. Large oxygen-containing species like CH_3OH, CH_3CHO, CH_3OCHO, CH_3OCH_3, and NH_2CHO, of compact ridge-type, show similar or slightly enhanced abundances in N as compared to M. The C_2H_5OH abundances are similar in N, M, and also in NW. The SO_2 and SO abundances in the M core (4×10^{-7} and 1×10^{-7}, respectively) are 13 and 5 times higher than in N and are very enhanced (10^3 and 10^2 times) as compared to NW. Such high SO_2 and SO abundances are also found in the prominent Orion A outflow source. In M the $SO^{18}O$ and $S^{18}O$ data suggest a $^{16}O/^{18}O$ ratio of 120. The $HOCO^+$ ion is detected in all three positions and appears to be 3 times more abundant in the NW position. $HCNH^+$ is seen only in NW.

Subject headings: Galaxy: center — ISM: abundances — ISM: individual (Sagittarius B2) — ISM: molecules — radio lines: ISM — surveys

1. INTRODUCTION

The Sgr B2 molecular cloud complex, located about 200 pc from the Galactic center at a distance of 8.5 kpc, contains $(5–10) \times 10^6\ M_\odot$ of gas of average density 2500 cm^{-3} in a region 45 pc (18′) in diameter (Scoville, Solomon, & Penzias 1975; Lis & Goldsmith 1989). About 10% of the gas resides in a north-south elongated core region $\sim 5 \times 10$ pc in size, where the density is $\sim 10^5$ cm^{-3} (Lis & Goldsmith 1991). In this core region high spatial resolution observations have revealed prominent compact hot cores of considerable chemical diversity (e.g., Goldsmith et al. 1987a; Vogel, Genzel, & Palmer 1987; Irvine, Goldsmith, & Hjalmarson 1987). The two most prominent cores are Sgr B2(N) and Sgr B2(M), separated by only 2 pc (∼48″), each containing

[1] Present address: Department of Physics, Rensselaer Polytechnic Institute, Troy, NY 12180.

some $10^4\ M_\odot$ of gas. Here the H_2 densities are as high as $10^7\ cm^{-3}$, and the average kinetic temperature increases from 20–40 K in the extended core to at least 80 K and 60 K for N and M, respectively, averaged over regions of 1 pc in size (21″ beam size) as estimated by Lis & Goldsmith (1991). At smaller scales (<21″) the temperature is likely to be higher (~150 K; see Vogel et al. 1987). Moreover, in parts of the extended envelope, there are indications of high gas kinetic temperatures presumably caused by shocks (Hüttemeister et al. 1993, 1995; Flower, Pineau des Forêts, & Walmsley 1995). However, here the considerably lower densities infer very subthermal excitation.

In the Sgr B2 core region a large variety of interstellar molecules have been identified (see Irvine, Goldsmith, & Hjalmarson 1987). There are two obvious reasons for the high detection rate of molecular lines: (1) the very large H_2 column density in this direction, $1.5 \times 10^{24}\ cm^{-2}$ averaged over a 45″ antenna beam and increasing to $11 \times 10^{24}\ cm^{-2}$ and $5 \times 10^{24}\ cm^{-2}$ across the central 0.1 pc (2″) N and M cores, respectively (e.g., Lis et al. 1993), and (2) the high core densities and kinetic temperatures readily produce sufficient collisional excitation of the rotational molecular lines. Moreover, as in other hot-core sources, sublimation of icy grain mantles and perhaps sputtering of refractory grains in these active regions drive a complex chemistry (see van Dishoeck & Blake 1998). Because of the complicated physical and kinematical structure of the cloud, in combination with the relatively low spatial resolution obtained with single-dish observations on account of its large distance, the spectral line profiles toward Sgr B2 are broad (10–20 km s^{-1}) and in many cases complicated. This makes line identification and interpretation of data cumbersome.

The earliest spectral line surveys of Sgr B2 (covering 72–115 GHz and 125–144 GHz) resulted in the detection of 457 lines from 39 molecular species (Cummins, Linke, & Thaddeus 1986) and (covering 70–115 GHz) more than 700 lines from 36 species (Turner 1989, 1991). Both surveys were pointed toward the Sgr B2(OH) position, located 30″ south of Sgr B2(M). The relatively large antenna beams (mean angular resolutions of 128″ and 83″, respectively) also sampled the emission from Sgr B2(M) but very little emission from Sgr B2(N). Sutton et al. (1991) surveyed the 330–355 GHz band toward Sgr B2(M) at 20″ angular resolution, resulting in 128 spectral lines from 22 molecules. They also made some comparison observations toward Sgr B2(N).

In this paper we present the first analysis of our three-position spectral line survey of Sgr B2 (Nummelin et al. 1998a, hereafter Paper I). The outline of this paper is as follows. In § 2 a brief summary of Paper I is given. In § 3 the method of data analysis is described, and in § 4 the resulting rotation temperatures and column densities are reported, together with a short discussion for each molecule. Finally, in § 5 we derive fractional abundances and discuss the physical and chemical characteristics of the three positions. We plan to present most of the chemical interpretation resulting from this analysis, as well as comparisons to other sources and to chemical models, in a subsequent paper.

2. THE LINE SURVEY DATA

The data analyzed in this paper were obtained from a spectral line survey covering the 218.30–263.55 GHz band made at approximately 23″ resolution using the 15 m Swedish-ESO Submillimetre Telescope (SEST[2]). The three positions[3] observed are the Sgr B2(N) and SgrB2(M) cores, and a position in the ambient cloud, Sgr B2(NW), 46″ west of Sgr 2(N). The latter position was chosen to sample cloud conditions where no signs of star formation are present, and where Nobeyama maps indicated a local column density peak (Ohishi 1992). In these data we detected 1730 lines from 40 species in the N core, 660 lines from 37 species in M, and 110 lines from 26 species toward the NW position. The complete spectrum with the proposed identification of each line can be found in Paper I, together with tabulations of the integrated line intensities and transition parameters for each molecule. Paper I also describes the details of the observations.

The same three positions in the Sgr B2 cloud have also been surveyed in the 30–50 and 70–116 GHz bands at the Nobeyama Radio Observatory (Ohishi, Ishikawa, & Kaifu 2000, in preparation). Our goal is to merge the SEST and Nobeyama data, obtained at similar angular resolutions, and in this way we hope to better investigate the physical and chemical hot core/ambient cloud structure already apparent from our SEST data, but where we suffer from a bias toward higher energy lines.

3. DATA ANALYSIS METHOD

In order to infer molecular excitation temperatures, column densities, and, subsequently, abundances relative to H_2 in a uniform way, two initial simplifying assumptions were made. These are (1) that the sources are homogeneous, and (2) that the excitation of any given molecular species is such that the relative distribution of the population over all of the energy levels can be described by a single Boltzmann temperature, referred to as the "rotational temperature" ($T_{\rm rot}$). The rotational temperatures may be different for different molecular species, and may or may not be a good approximation to the gas kinetic temperature. This will be discussed further in § 5. Under these assumptions, the antenna main-beam brightness temperature ($T_{\rm mb}$) can be expressed as

$$T_{\rm mb} = \eta_{\rm bf}[J_\nu(T_{\rm rot}) - J_\nu(T_{\rm bg})](1 - e^{-\tau_{ul}})\ , \qquad (1)$$

where

$$J_\nu(T) = \frac{h\nu_{ul}}{k}\,\frac{1}{e^{h\nu_{ul}/kT} - 1}\ , \qquad (2)$$

and where h is Planck's constant, k is Boltzmann's constant, and ν_{ul} is the frequency of the $u \rightarrow l$ transition. The "beam-filling factor," $\eta_{\rm bf}$, is defined as

$$\eta_{\rm bf} = \frac{\Omega_{\rm s}}{\Omega_{\rm s} + \Omega_{\rm mb}}\ , \qquad (3)$$

where $\Omega_{\rm s}$ and $\Omega_{\rm mb}$ are the sky solid angles subtended by the source and the antenna main beam, respectively. In equation (3) it is assumed that both the source structure and the beam shape are Gaussians. The temperature of the background radiation, $T_{\rm bg}$, was set to 2.73 K throughout the

[2] The Swedish-ESO Submillimetre Telescope is operated jointly by ESO and the Swedish National Facility for Radio Astronomy, Onsala Space Observatory, at Chalmers University of Technology.

[3] Source coordinates given in Table 1.

analysis, although its influence is negligible when $T_{\rm rot} \gg 2.7$ K. Similarly, the background radiation in the 1 mm band from continuum and hot dust sources is neglected, but, of course, radiation from hot dust could affect $T_{\rm rot}$ via infrared or near-infrared transitions. Assuming that the line has a Gaussian shape, the optical depth at the center of a line, τ_{ul}, can be calculated through

$$\tau_{ul} = \sqrt{\frac{\ln 2}{16\pi^3}} \frac{c^3 A_{ul} g_u N}{\nu_{ul}^3 Q(T_{\rm rot}) \Delta V} e^{-E_u/kT_{\rm rot}} (e^{h\nu_{ul}/kT_{\rm rot}} - 1) , \quad (4)$$

where c is the speed of light, A_{ul} is Einstein's coefficient for spontaneous radiative decay, g_u is the statistical weight of the upper state, N is the total molecular column density, $Q(T_{\rm rot})$ is the molecular partition function evaluated at a temperature $T_{\rm rot}$, ΔV is the full velocity width at FWHM of the spectral line, and E_u is the energy above ground of the upper state of the transition.

Given the free parameters $\eta_{\rm bf}$, $T_{\rm rot}$, and N, the integrated line intensity can be calculated through equations (1)–(4). Throughout these calculations, the average line widths for each source was used as ΔV, i.e., 13 km s^{-1}, 17 km s^{-1}, and 14 km s^{-1}, were used for Sgr B2(N), Sgr B2(M), and Sgr B2(NW), respectively. The set of input parameters producing the closest match to the full set of observed line intensities for each molecular species, the "best-fit model," was obtained by finding the minimum of the reduced χ^2 function (χ_ν^2). This is defined as

$$\chi_\nu^2 = \frac{1}{n-p} \sum_{i=1}^{n} \left(\frac{I_i^{\rm obs} - I_i^{\rm calc}}{\sigma_i^{\rm obs}} \right)^2 , \quad (5)$$

where n is the number of data points, p is the number of free parameters, $I_i^{\rm obs}$ is the observed integrated line intensity, $I_i^{\rm calc}$ is the integrated line intensity calculated from equations (1)–(4), and $\sigma_i^{\rm obs}$ is the 1 σ uncertainty of the observed line intensity. Some species exhibit asymmetric line profiles, mainly in the low-energy lines, in M and N. Furthermore, several of the species observed in the NW position, e.g., HNCO and CH_3OH, have lines with multiple velocity components. However, we have consequently used the total integrated line intensity throughout the analysis (the quantities tabulated in Paper I). The reason is that in the hot core sources, M and N, the line crowding is generally too severe to allow a reliable multiple Gaussian fit to the asymmetric line profiles. In NW the signal-to-noise (S/N) ratio is often too poor to allow for an accurate analysis of multiple velocity components. A systematic uncertainty of 30% was used for all observed line intensities to account for possible errors in pointing and calibration.

A consequence of using the χ^2-value as the goodness-of-fit indicator is that solutions producing $I_i^{\rm calc} < I_i^{\rm obs}$ are somewhat favored compared to those producing $I_i^{\rm calc} > I_i^{\rm obs}$ (as was discussed in Nummelin et al. [1998b]). Therefore, the column densities obtained in this way are, as a whole, slightly lower than what would have been obtained through, e.g., least-squares fits in the logarithmic "rotation diagrams" (see below). For a few of the analyzed molecular species, e.g., CH_3CHO, NH_2CHO, and CH_3OCHO, the actual minimum χ^2 was obtained for a combination of $\eta_{\rm bf}$ and N that was considered unphysical (i.e., highly inconsistent with other observations), in which case that model was rejected.

The right panel of Figure 1 shows an example of χ_ν^2 as a function of the rotation temperature and column density. The contours indicated in the plot are

$$\chi_\nu^2 \le \chi_{\nu,\rm min}^2 + \frac{\Delta\chi^2}{n-p}$$

for $\Delta\chi^2$ values equal to 2.3, 4.6, 9.2, and 13.8. Assuming that the model describes the physics adequately and that all measurements are distributed according to the normal distribution, the probability of enclosing the true parameters $T_{\rm rot}$ and N is 68.3% ($\approx 1\ \sigma$), 90%, 99%, and 99.9%, for each of the $\Delta\chi^2$ values, respectively (Lampton, Margon, & Bowyer 1976).

In most cases the beam-filling factor, $\eta_{\rm bf}$, could not be directly estimated from the data and was therefore set to unity. This means that the column density and rotation temperature deduced will be a beam-averaged (over the 23″ beam) quantity. However, for a number of species we found

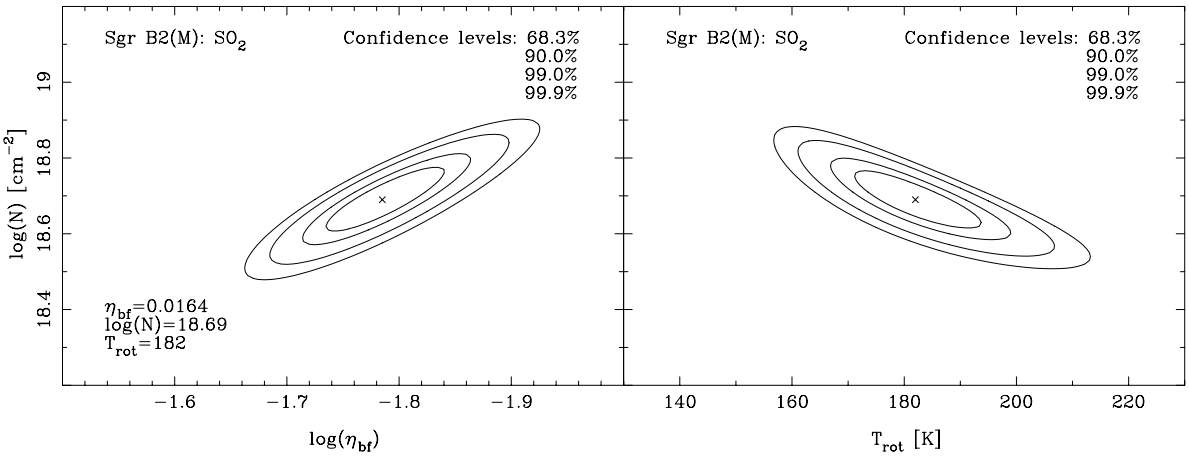

FIG. 1.—Contours of constant χ_ν^2 value (the goodness-of-fit) over the parameter space spanned by the beam-filling factor ($\eta_{\rm bf}$) and column density (N) (*left panel*), and by the rotation temperature and column density (*right panel*). A cross marks the best-fit parameters (giving the smallest χ_ν^2) in each of the panels. In the left panel the rotation temperature is not a free parameter, but is fixed at 182 K, and because of this the confidence regions are only approximate.

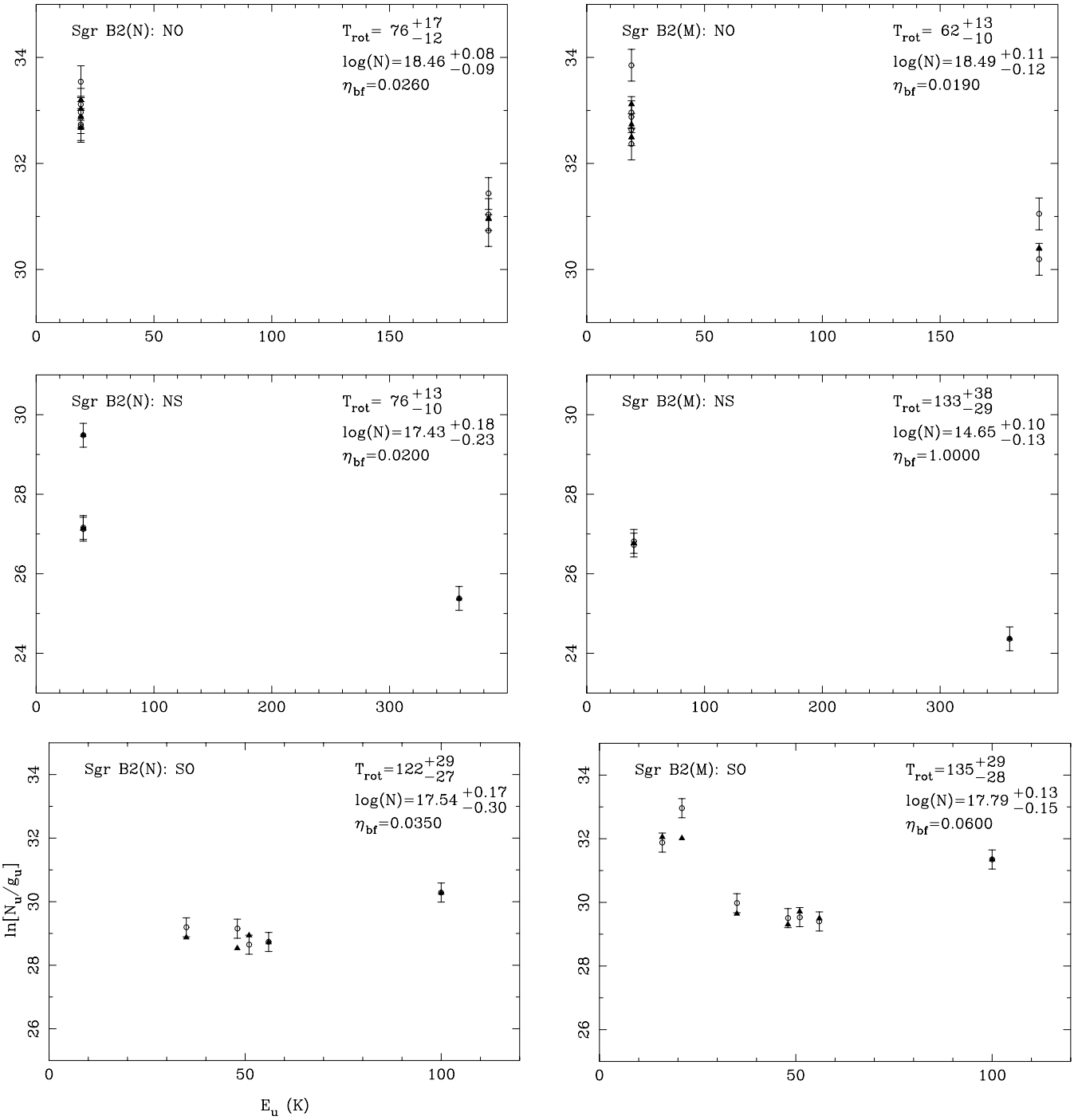

FIG. 2.—In these rotation diagrams the observed line intensities are plotted (*circles*) together with the intensities resulting from the best-fit model (*triangles*). The error bars indicate 30% pointing and calibration uncertainty. Transitions suspected to be significantly blended with other species have been excluded.

the best fit to the data to be obtained for a beam-filling factor $\ll 1$. These molecules are by no means unique, being highly localized, whereas the rest of the molecules have extended emission. The difference is rather that only in these cases could line optical depths be securely constrained through the relative intensities of observed lines. This also constrains the molecular column density through equation (4), which in turn constrains the beam-filling factor. A requirement to obtain a significant improvement in the goodness-of-fit to the data by allowing small beam-filling factors is that transitions with both large and small A-coefficients have been observed. We considered a beam-filling value less than 1 to be statistically significant only if it improved the χ^2_ν more than 1 σ. An illustration of the contours of constant χ^2_ν as a function of η_{bf} and the column density in the case of SO_2 can be found in the left panel of Figure 1.

The observational data and the intensities resulting from the best-fit models for each species were, subsequent to the χ^2-analysis, presented in the population or "rotation"

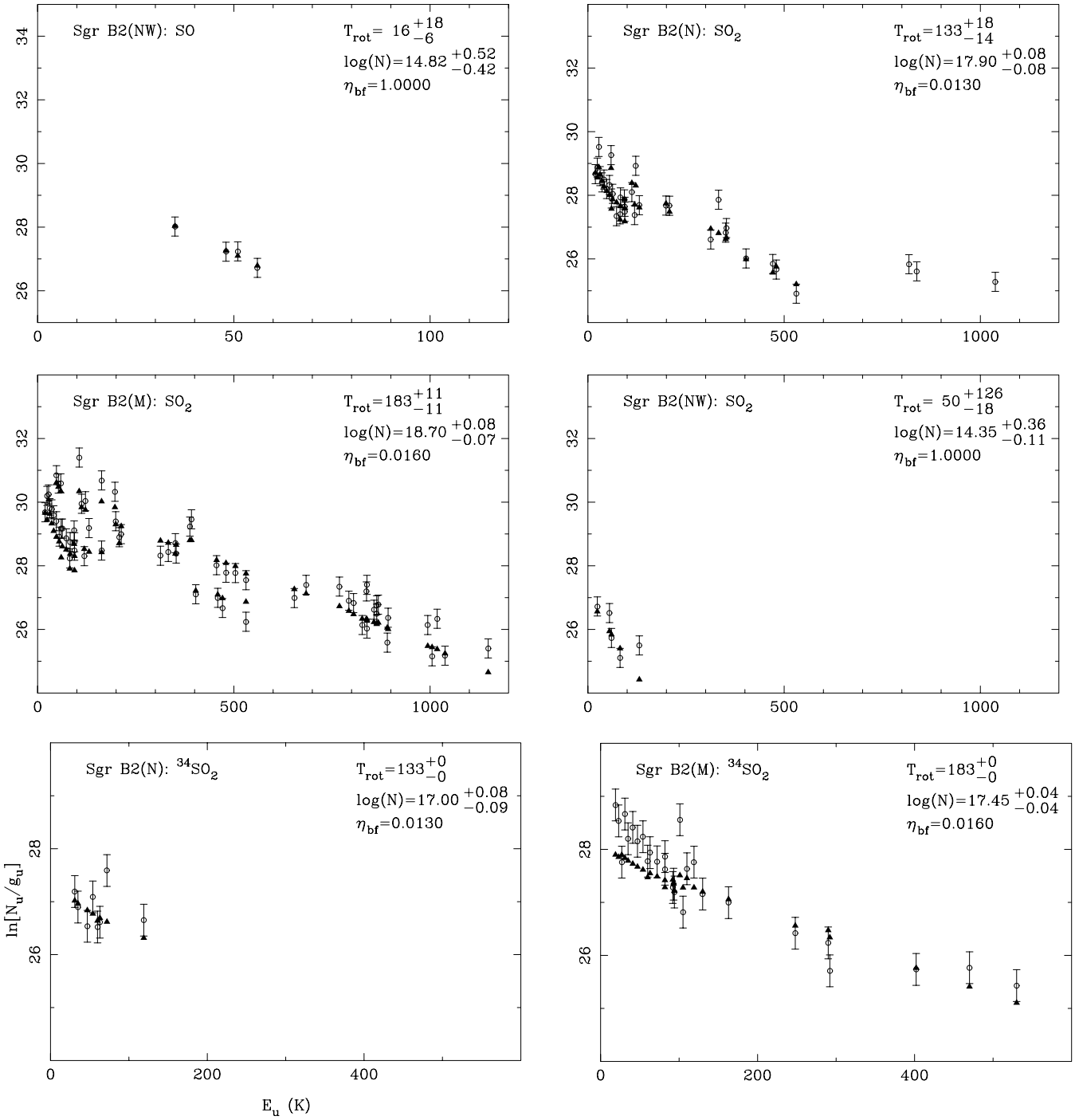

FIG. 2.—*Continued*

diagram format, in which the quantity

$$\ln\left(\frac{8\pi k\nu_{ul}^2}{hc^3 A_{ul}\, g_u}\int T_{\rm mb}\, dv\right) = \ln\left(\frac{N_u}{g_u}\right), \qquad (6)$$

where N_u is the column density of molecules in the upper state, is plotted as a function of the upper-state energy (E_u). Under the assumptions of Boltzmann-distributed level populations, a homogeneous source with equal beam-filling for all transitions, optically thin emission, and negligible background radiation the plotted data points will fall along a straight line. In that case, the inverse of the negative slope of a line fitted to the data is equal to the rotational temperature. As is immediately clear from the scattered appearance of most of the rotation diagrams in Figure 2, the above simplifying assumptions are not strictly fulfilled in Sgr B2. A thorough and illuminating discussion of the rotation diagram method is given by Goldsmith & Langer (1999).

Two exceptions to the analysis method described above are HC_3N and CH_3OH, for which somewhat modified methods were used (see § 4.29 and 4.30).

Beam-averaged column densities of molecules for which no rotation temperatures could be determined, i.e., molecules detected either through a single transition or through

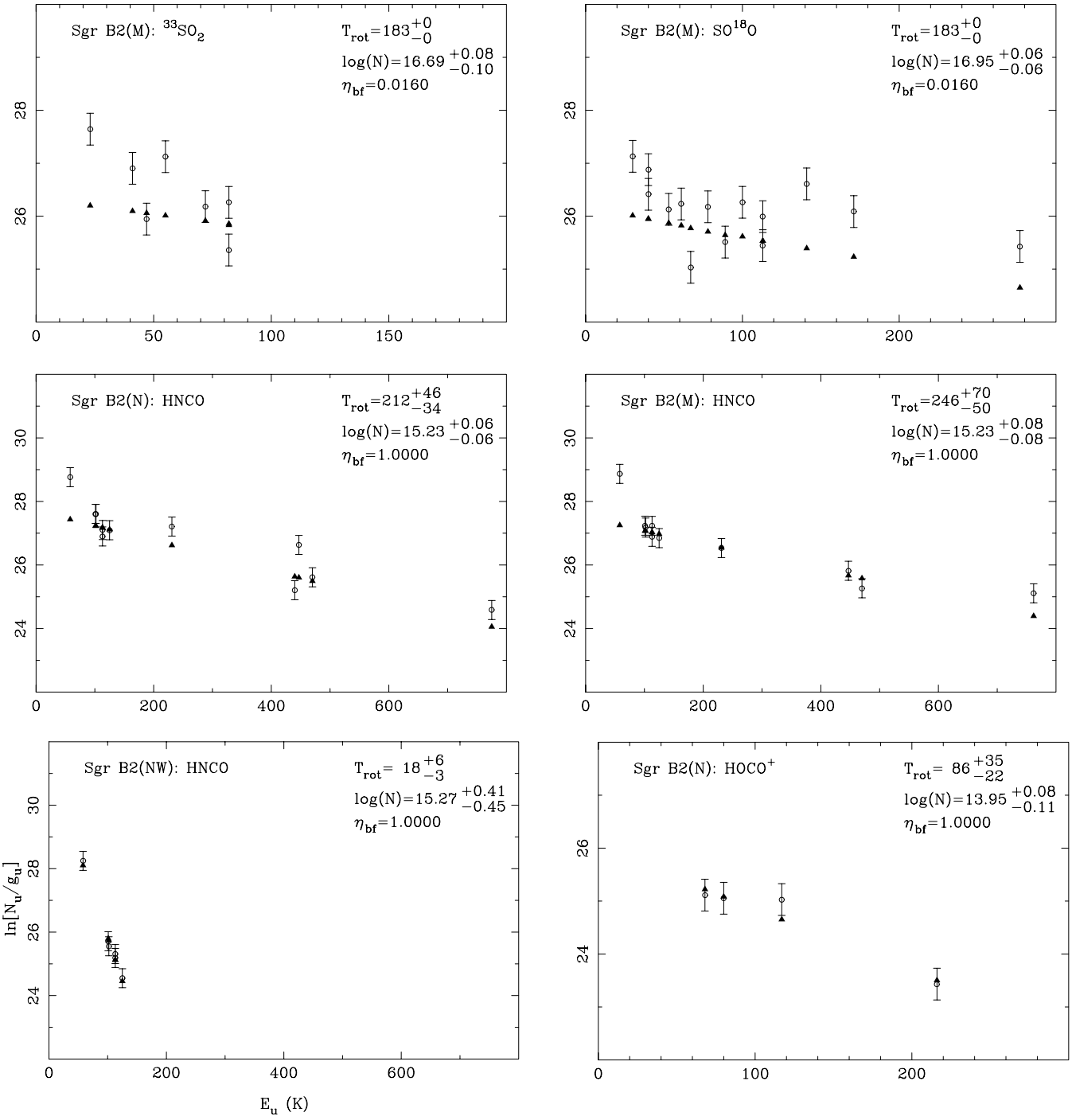

FIG. 2.—*Continued*

transitions having nearly the same upper-state energies, were calculated through

$$N = \frac{8\pi k}{hc^3}\,\frac{v_{ul}^2\,Q(T_{\rm rot})}{A_{ul}\,g_u}\,e^{E_u/kT_{\rm rot}}\int T_{\rm mb}\,dV\ , \qquad (7)$$

where optically thin emission ($1 - e^{-\tau_{ul}} \approx \tau_{ul}$) and negligible background radiation have been assumed in addition to the previous assumptions. For these molecules rotation temperatures of 50 K for Sgr B2(N) and Sgr B2(M), and 20 K for Sgr B2(NW) were assumed. These assumptions are, in part, based on the HC_3N results of Lis & Goldsmith (1991). They obtained 20–40 K on the 10 pc scale, while around the M and N cores they derived kinetic temperatures of 60 and 80 K, respectively. Guided by the dust temperature model of Zmuidzinas et al. (1995) we adopted slightly lower values. However, the resulting column density is rather insensitive to changes in $T_{\rm rot}$. From equation (7) we find that

$$\delta N/N = (\alpha - E_u/kT_{\rm rot})\delta T_{\rm rot}/T_{\rm rot}\ , \qquad (8)$$

where $\alpha = 1$ for diatomic and linear molecules. In the case of more complicated molecules $\alpha = 3/2$. Since E_u/k often is a fair fraction of $T_{\rm rot}$ a certain relative uncertainty in rotation temperature, $\delta T_{\rm rot}/T_{\rm rot}$, yields about the same (or less) rela-

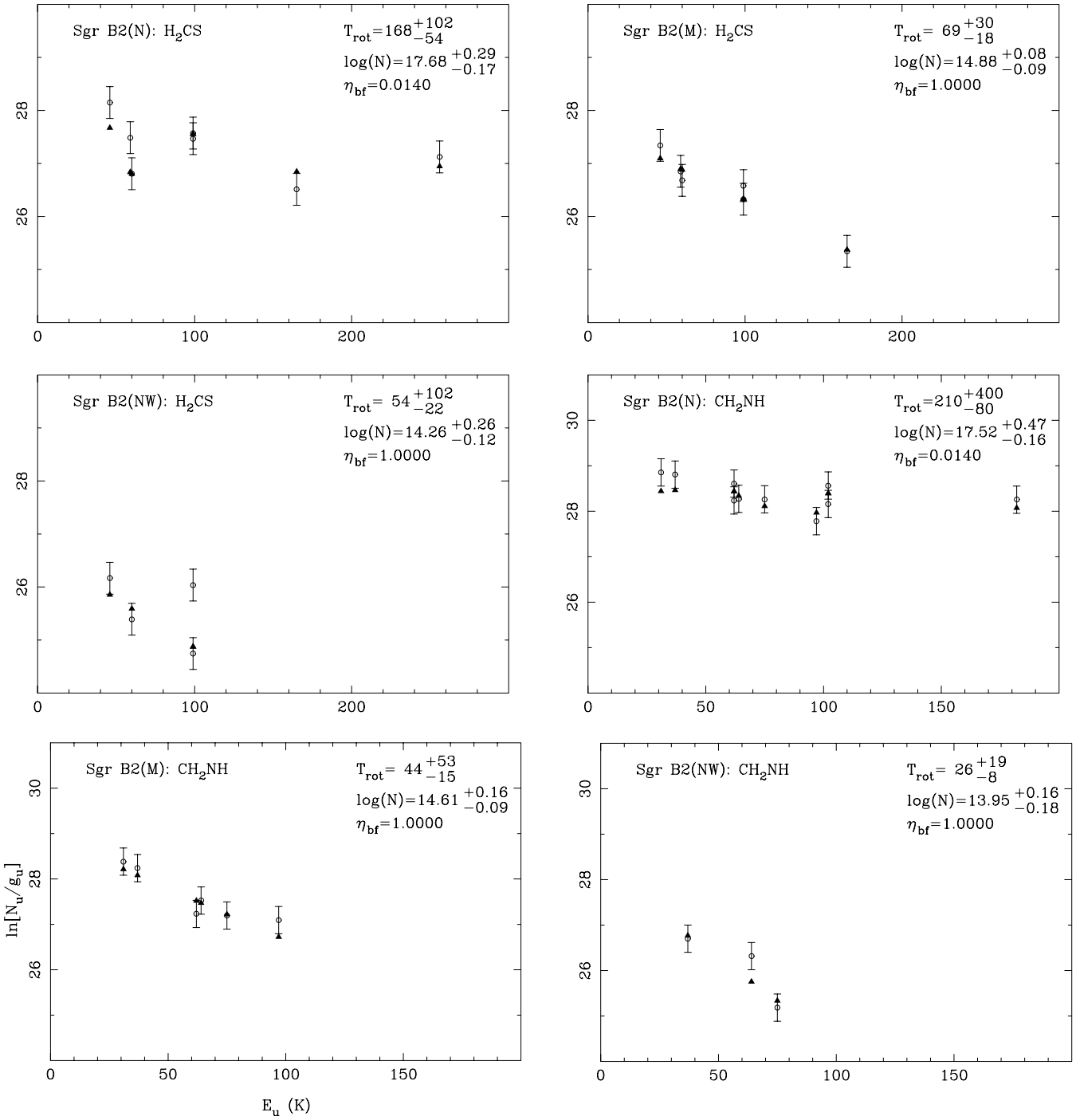

FIG. 2.—*Continued*

tive uncertainty, $\delta N/N$, in the derived column density. Uncertainties due to optically thick line emission are likely to be larger and column densities derived with equation (7) should probably overall be treated as lower limits.

In the calculation of the rotational partition functions we have used the approximate analytical expressions given by Blake et al. (1987) and Turner (1991). In a few cases where there is significant population in excited vibrational states, we have also included the vibrational partition functions.

4. RESULTS

In this section we report the results obtained for each molecule, in order of increasing molecular complexity. By convention, the chemical symbol of the main isotopomer of each species is written without atomic weights throughout this paper, except where needed for clarity.

The results are summarized in Table 1 (rotation temperatures, column densities, and beam-filling factors), Table 2 (isotopomeric column density ratios), and Table 3 (fractional abundances). The error limits given in Table 1 are the boundaries of the $\Delta\chi^2 < 2.3$ region in the ($T_{\rm rot}$, N) parameter space, i.e., approximately 1 σ errors. These errors do not include the uncertainty in column density or rotation temperature due to the uncertainty in the beam-filling factor. For references to earlier molecular line observations see Turner (1991).

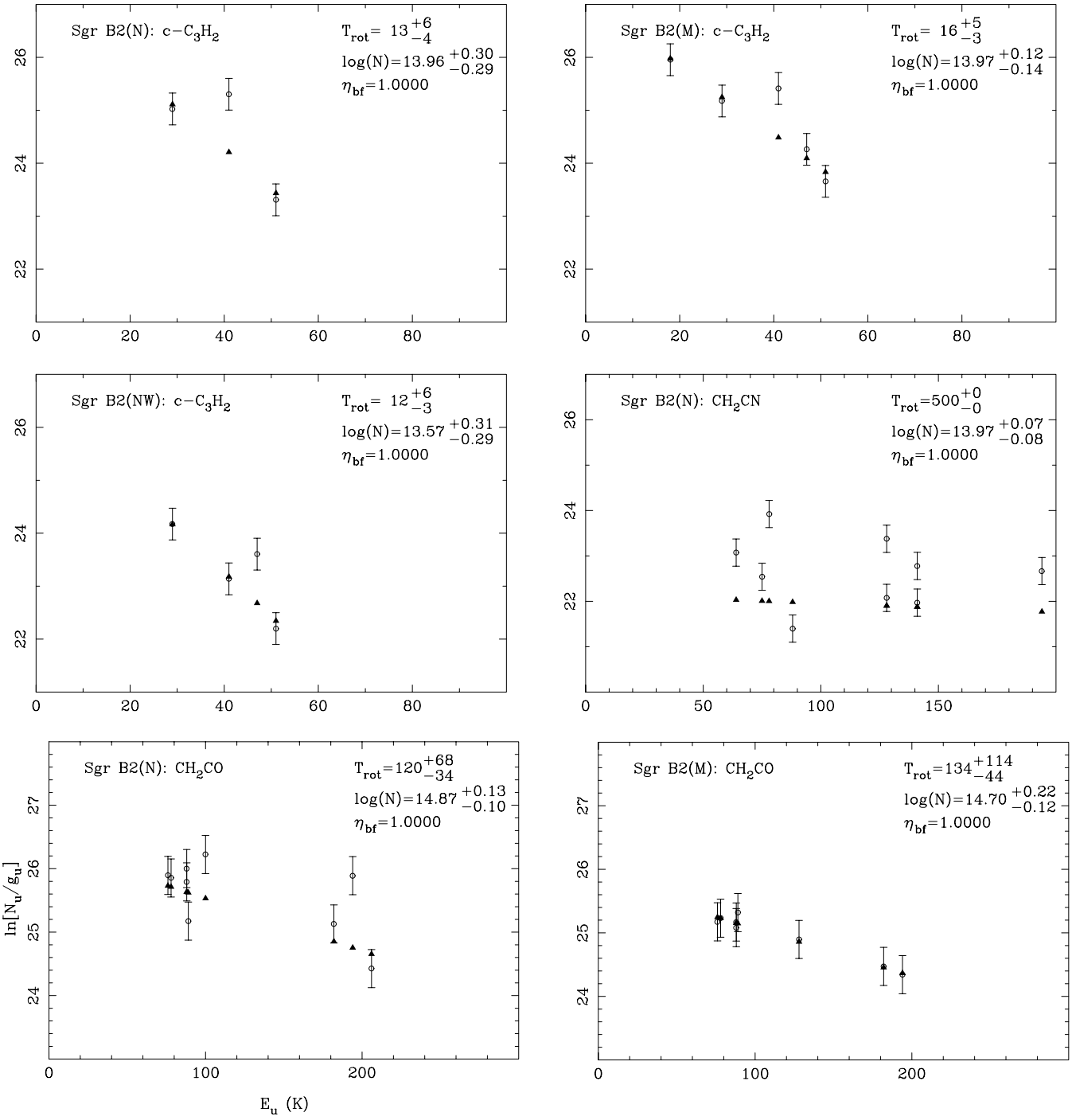

FIG. 2.—*Continued*

Rotation diagrams can be found in Figure 2. In the analysis we have excluded transitions which in Paper I were regarded as ambiguously identified or severely blended.

4.1. CN

The $J = 2 \rightarrow 1$ transition of the cyanide radical, CN, was detected through two extremely blended bands of absorption and emission lines around 226–227 GHz. The identification of individual hyperfine-component lines is impossible since the emission/absorption occurs at different velocities, and also because the CN emission may be more extended than the separation of the signal and reference beams, which would lead to subtraction of off-source emission from the on-source spectra. Therefore, no detailed analysis has been made of the CN ($J = 2 \rightarrow 1$) band. However, it is likely that the optical depths of the strongest CN transitions are at least of order unity in the low excitation gas in front of the continuum sources in Sgr B2(N) and Sgr B2(M), since the continuum emission is almost completely absorbed.

4.2. CO

No useful data were obtained from the main isotopomer of carbon monoxide, CO, since the CO ($J = 2 \rightarrow 1$) emission in Sgr B2 is more extended than the separation of the signal and reference beam in the beam-switch mode used during

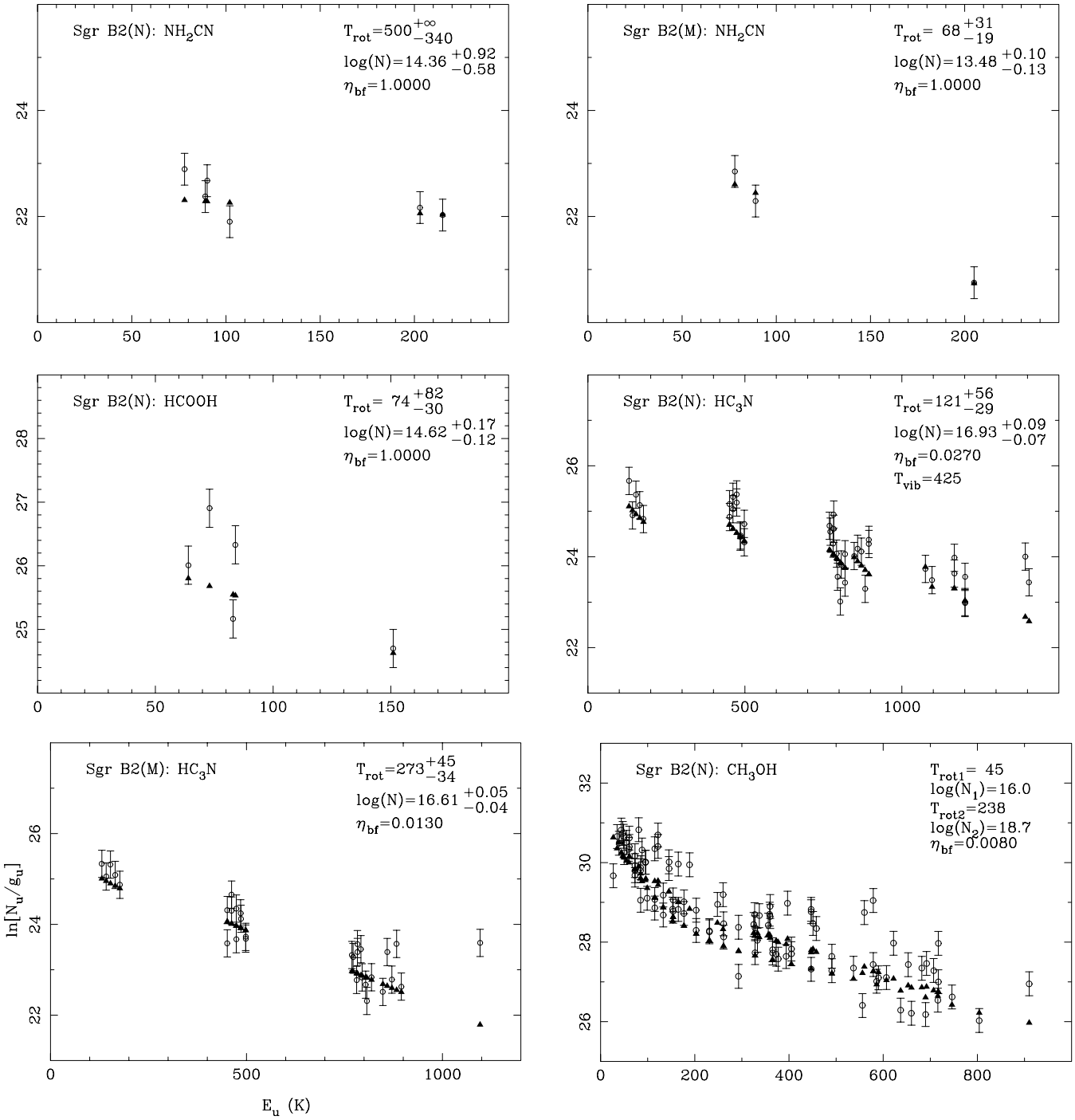

FIG. 2.—*Continued*

the observations, and since the emission probably also is affected by absorption in foreground gas. This is also the case for ^{13}CO. For $C^{17}O$, the column densities become 4.7×10^{16} cm^{-2}, 6.0×10^{16} cm^{-2}, and 9.5×10^{15} cm^{-2} toward the N, M, and NW positions, respectively. Because $C^{17}O$ is the least abundant CO isotopomer observed, and the $C^{17}O$ $J = 2 \rightarrow 1$ line therefore is the least saturated one, it was used to estimate the H_2 column density (see § 5.1). The increasing $C^{18}O/C^{17}O$ column density ratio going from N to M and NW probably reflects a decreasing optical depth in the $C^{18}O$ line.

Both the $C^{18}O$ and $C^{17}O$ lines show some velocity structure. In N the peak of the $C^{18}O$ line occurs at $V_{LSR} = 69$ km s^{-1} while there is a wing component around 93 km s^{-1}. In M there is a distinct, broad ($\Delta V = 35$ km s^{-1}) wing feature at 75 km s^{-1}, in addition to the main line component centered at 58 km s^{-1}. Toward NW there are two clearly resolved components at 120 and 94 km s^{-1}, apart from the main line at 67 km s^{-1}. The $C^{17}O$ line is centered at 67 km s^{-1} in N and has irregular shape but no resolvable velocity components. In M, on the other hand, there is a wing at 84 km s^{-1}, while the main component is centered at 60 km s^{-1}. In NW the $C^{17}O$ line has one dominant component at 69 km s^{-1}, although a very weak feature can be seen around 100 km s^{-1}. Toward N and M there is also absorption of the continuum at around $V_{LSR} = -40$ km s^{-1}

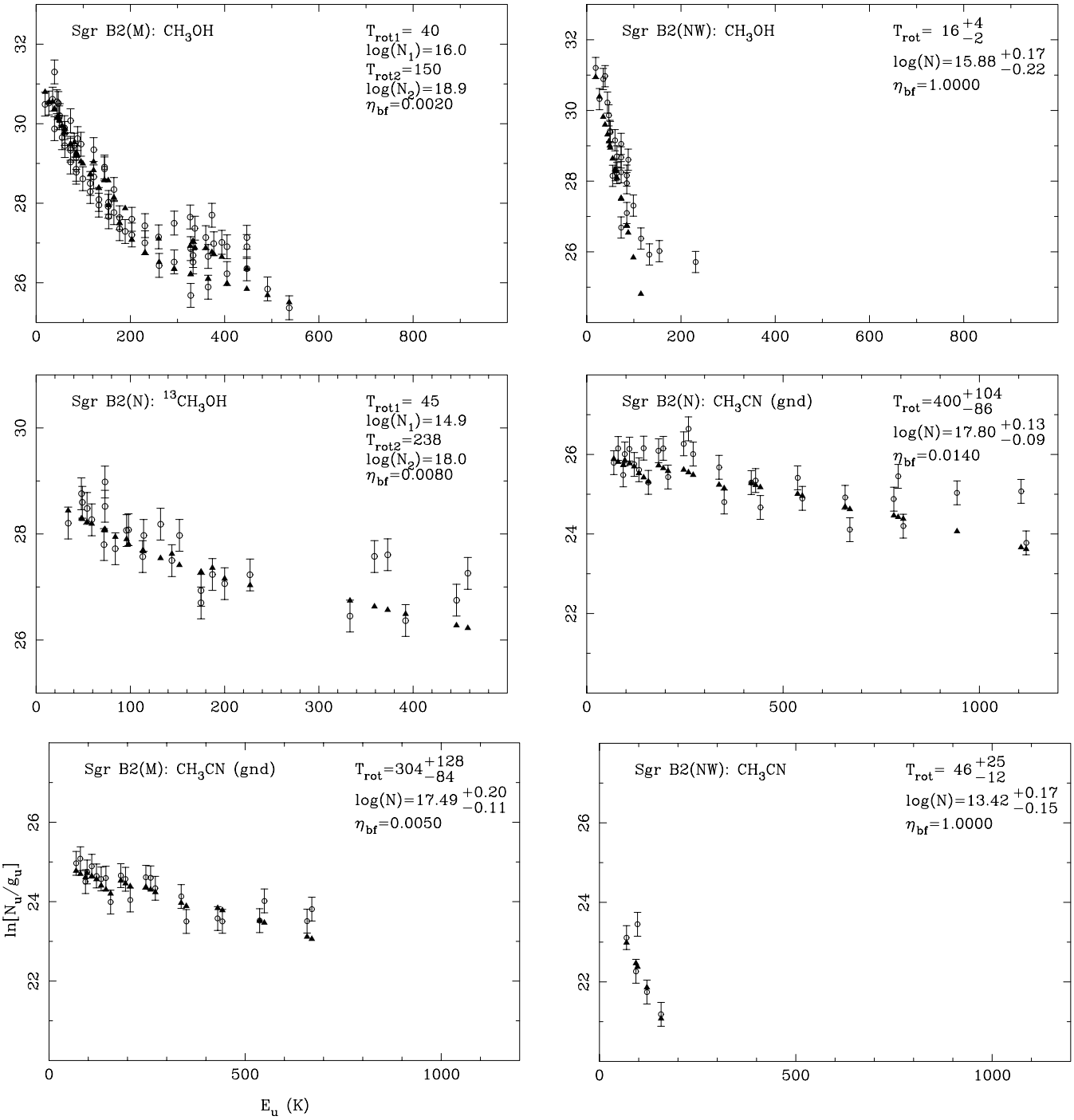

FIG. 2.—*Continued*

caused by $C^{18}O$ in the foreground spiral arm gas, in good agreement with the results by Greaves & Nyman (1996).

4.3. CS

The observed $J = 5 \rightarrow 4$ transition of carbon monosulfide, CS, suffers from prominent self-absorption in N and M, and therefore cannot be treated with the homogeneous, uniform excitation model used here. The line feature seen toward NW, with the main component at 55 km s^{-1} and a wing at 77 km s^{-1}, probably results from a combination of self-absorption on the high-velocity side of the peak, and emission from two velocity components. The column density in NW becomes 4.4×10^{14} cm^{-2}.

The rarer isotopomer $C^{34}S$ was detected in all three positions, yielding column densities of 1.9×10^{14} cm^{-2}, 2.1×10^{14} cm^{-2}, and 4.3×10^{13} cm^{-2} toward N, M, and NW. The $C^{32}S/C^{34}S$ column density ratio in NW is 10. Moreover, ^{13}CS was detected in N and M (the ^{13}CS band was not covered toward NW), and the resulting column densities are 2.0×10^{14} cm^{-2} and 2.1×10^{14} cm^{-2}, respectively. $C^{33}S$ was also detected in N and M, yielding column densities of 3.4×10^{13} cm^{-2} and 6.4×10^{13} cm^{-2}, respectively. The $^{13}C^{34}S$ isotopomer was detected in all three positions (toward NW during later, dedicated observations of CS in Sgr B2), although we suspect that, at least in N, this line is blended with the $9_0 \rightarrow 8_0$ line of the *E* species of

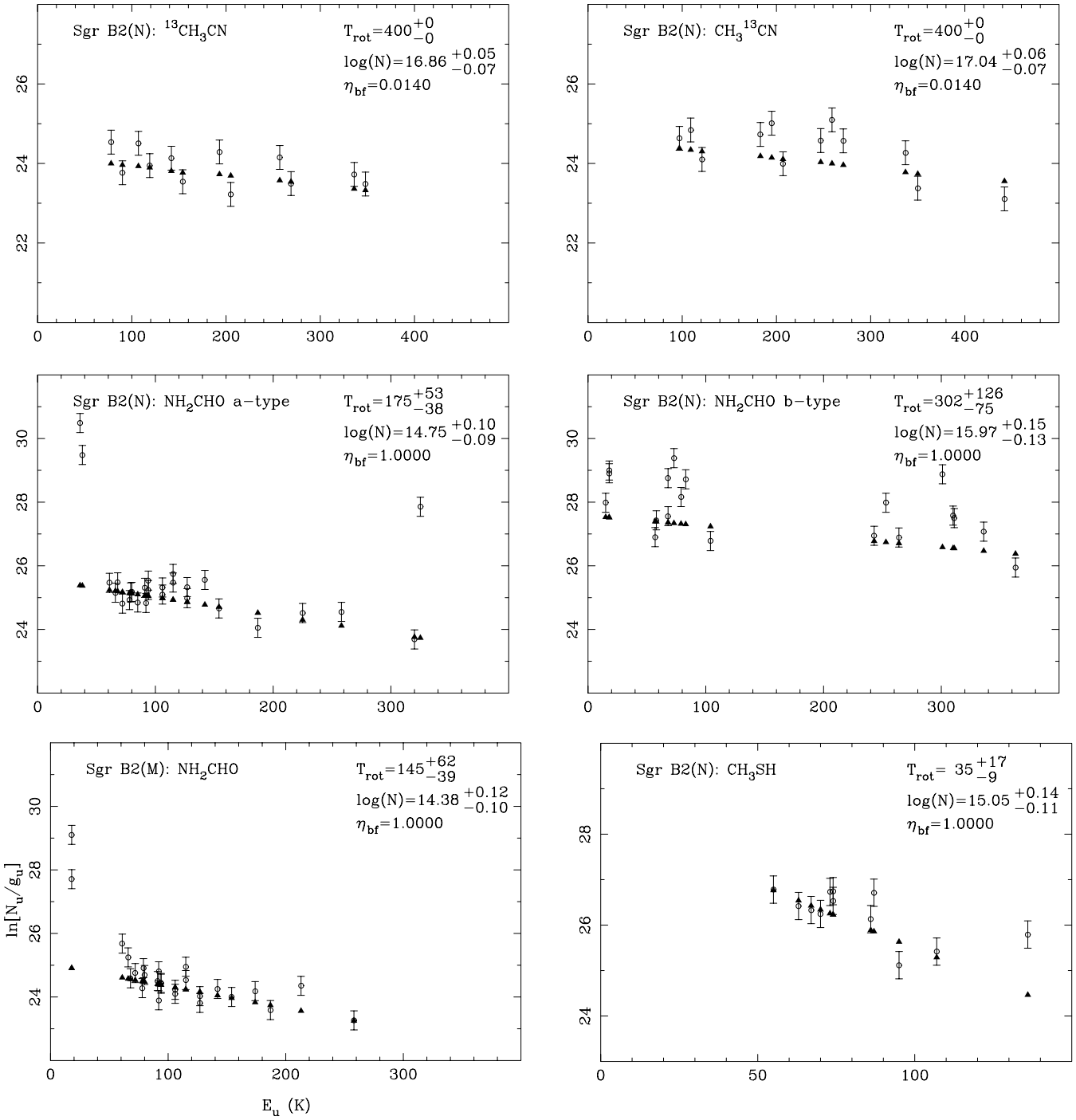

FIG. 2.—*Continued*

CH_3SH. The column densities become 4.2×10^{13} cm^{-2}, 3.5×10^{13} cm^{-2}, and 7.6×10^{12} cm^{-2} in N, M, and NW, respectively.

The $^{13}CS/^{13}C^{34}S$ and $C^{34}S/^{13}C^{34}S$ column density ratios are both similarly low and about 5 in N and 6 in M, which probably results from a combination of a blend of the $^{13}C^{34}S$ line with CH_3SH and high optical depths in ^{13}CS and $C^{34}S$. Also in NW the $C^{34}S/^{13}C^{34}S$ ratio is low, about 6.

4.4. SiO

Silicon monoxide (SiO) has one transition, $J = 6 \rightarrow 5$, in the observed band. In N the main velocity component is centered at 67 km s^{-1}, while there is a broad additional feature around 85 km s^{-1}. The column density becomes 6.8×10^{13} cm^{-2}. In M the line is somewhat self-absorbed and also extends to high velocities ($V_{LSR} \sim 115$ km s^{-1}). The column density, 9.6×10^{13} cm^{-2}, is probably somewhat underestimated owing to the self-absorption. In NW the column density becomes 2.0×10^{13} cm^{-2}.

In addition to the main isotopomer (^{28}SiO), the less abundant variants ^{29}SiO and ^{30}SiO were detected in M, and the $^{29}SiO/^{30}SiO$ column density ratio is 2.0 ± 0.8. The $^{28}SiO/^{29}SiO$ column density ratio of 11 should be considered a lower limit to the actual value, because of the self-absorption in ^{28}SiO.

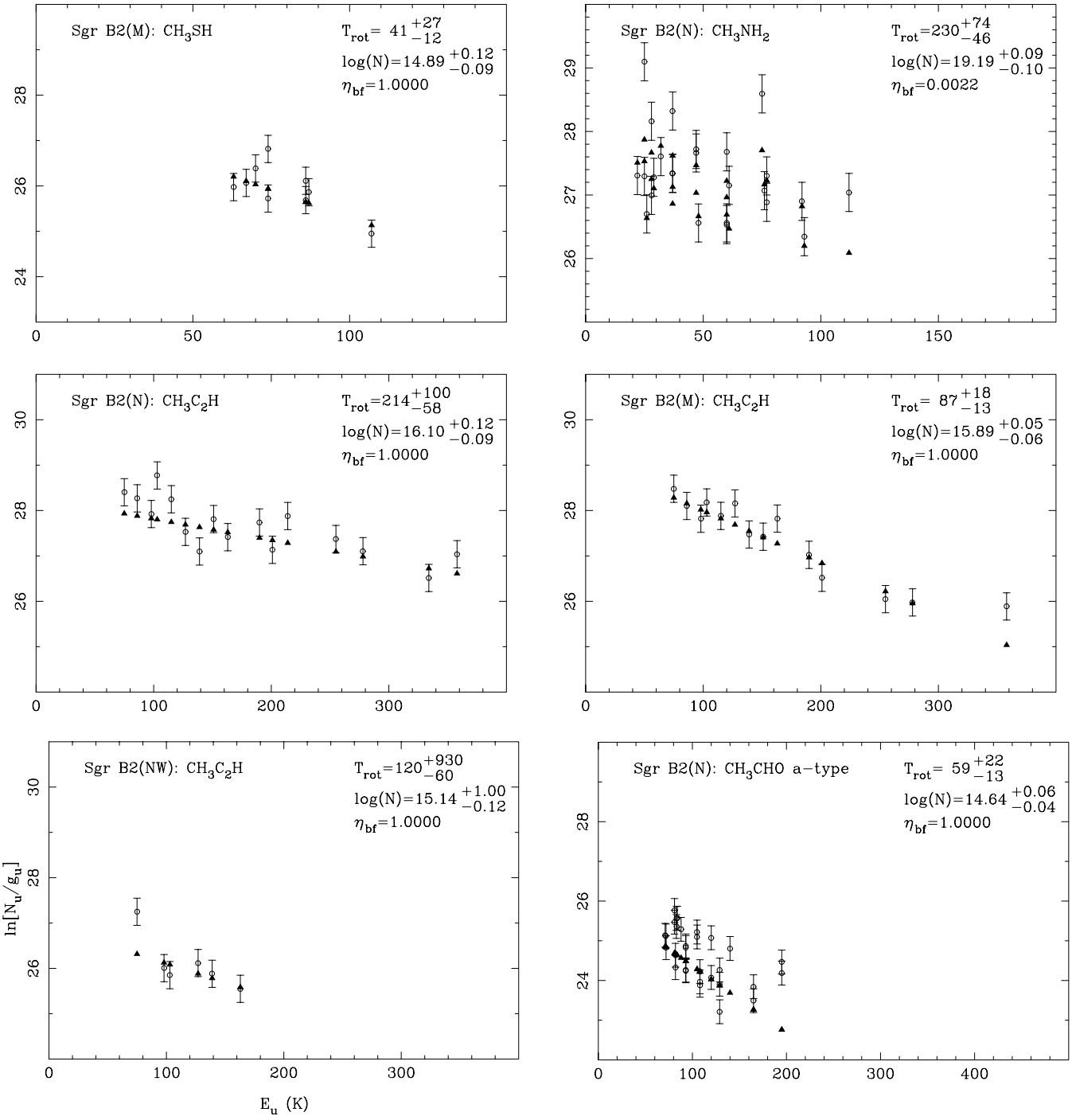

FIG. 2.—*Continued*

4.5. NO

The nitrogen oxide radical, NO, was detected toward N and M through the $J = 5/2 \rightarrow 3/2$ rotational transition in both the $^2\Pi_{1/2}$ and $^2\Pi_{3/2}$ states, each of which has several resolved hyperfine components. This allowed a rotation temperature to be determined, on the assumption that the cross-state temperature also characterizes the rotational temperatures within each state. The detection of several resolved hyperfine components allowed the optical depths to be determined. In both N and M an improvement greater than 1 σ in the χ_ν^2 was obtained for low beam-filling factors, 0.026 (3″.8) and 0.019 (3″.2), respectively. The ability to determine the optical depths of the observed NO transitions here relies on the detection of the intrinsically weaker $\Delta F = 0$ line components in the $^2\Pi_{1/2}$ state, and the peak optical depths in the best-fitting models are between 1 and 2 in both cores. The rotation temperatures become 76 and 62 K, and the column densities are 2.9×10^{18} cm^{-2} and 3.1×10^{18} cm^{-2} for N and M, respectively. In NW the beam-averaged column density is 1.0×10^{16} cm^{-2} for an assumed rotation temperature of 20 K.

4.6. NS

Toward the N and M positions the nitrogen sulfide radical, NS, was detected through lines in both the $^2\Pi_{1/2}$ and $^2\Pi_{3/2}$ states, which enabled rotation temperatures to be

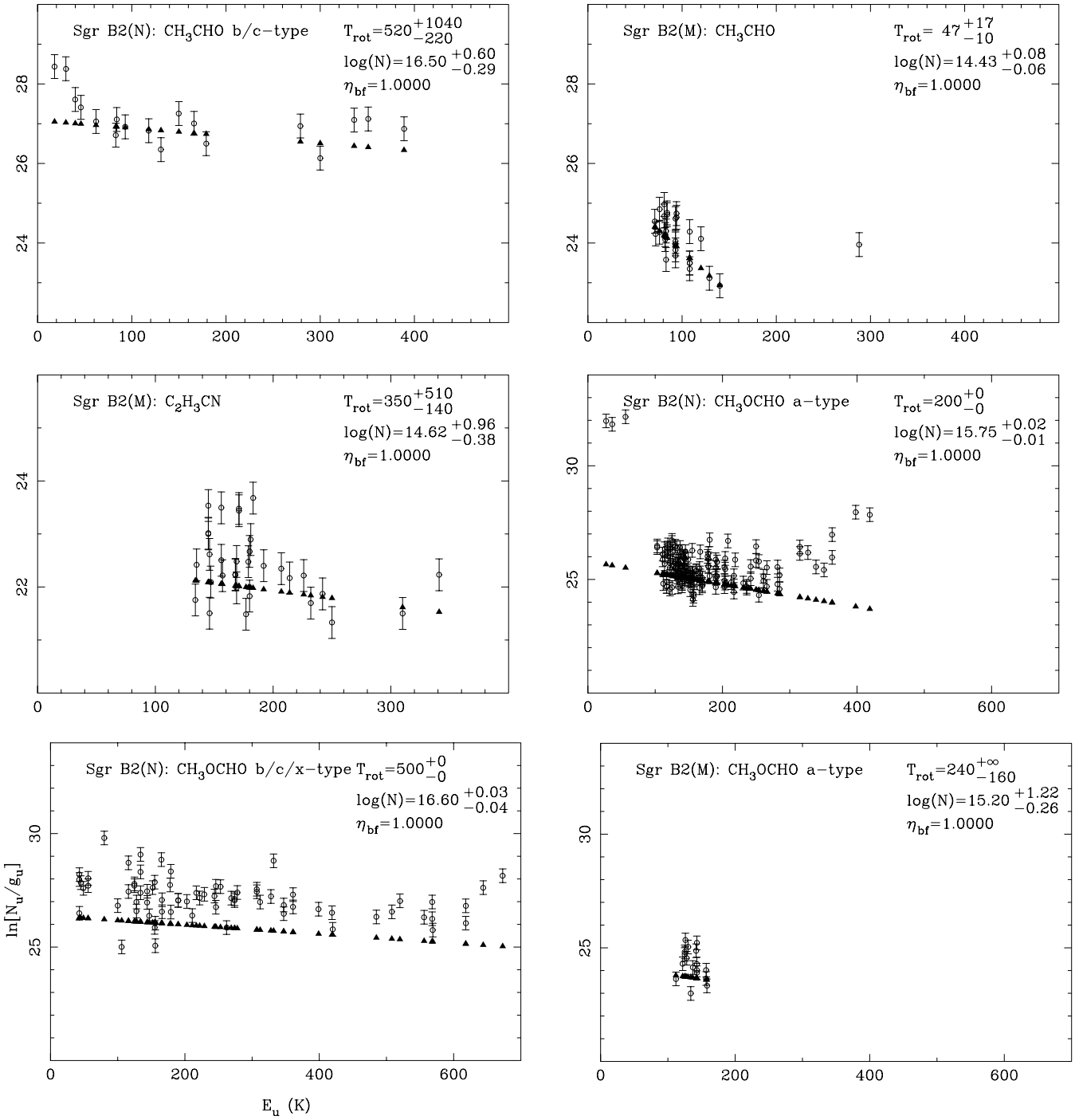

FIG. 2.—*Continued*

determined under the same assumptions as for NO. In N a small beam-filling, 0.020 (3″), fits the data, and the corresponding rotation temperature and column density become 76 K and 2.7×10^{17} cm^{-2}, respectively. In this model the optical depths in the $^2\Pi_{1/2}$ transitions (with high A-coefficients) become rather high, about 13. Although the low beam-filling factor is statistically well determined by the data, it relies exclusively on the detection of the $^2\Pi_{1/2}$ $J = 11/2 \rightarrow 9/2$ $\Delta F = 0$ hyperfine components around 253.61 GHz, which have lower A-coefficients. However, this line doublet is overlapping the HC^{13}CCN ($J = 28 \rightarrow 27$) line and the intensity could therefore be somewhat uncertain. By ignoring the $\Delta F = 0$ lines and setting the beam-filling equal to unity, a rotation temperature of 179 K and a column density of 9.1×10^{14} cm^{-2} are obtained. However, we note that the small beam-filling is similar to that deduced for NO.

In M the $\Delta F = 0$ lines were not detected and, hence, no optical depths could be determined. The best-fitting rotation temperature is 133 K, and the beam-averaged column density is 4.5×10^{14} cm^{-2}. However, a beam-filling factor could be estimated in the following way. Toward N, both the rotation temperatures and beam-filling factors of NO and NS are similar. If we assume that this similarity is not a coincidence, and therefore set the rotation temperature of NS toward M to be identical to that of NO, 62 K, the best fit to the data is obtained for a beam-filling factor of 0.013 and a column density of 3.4×10^{17} cm^{-2}.

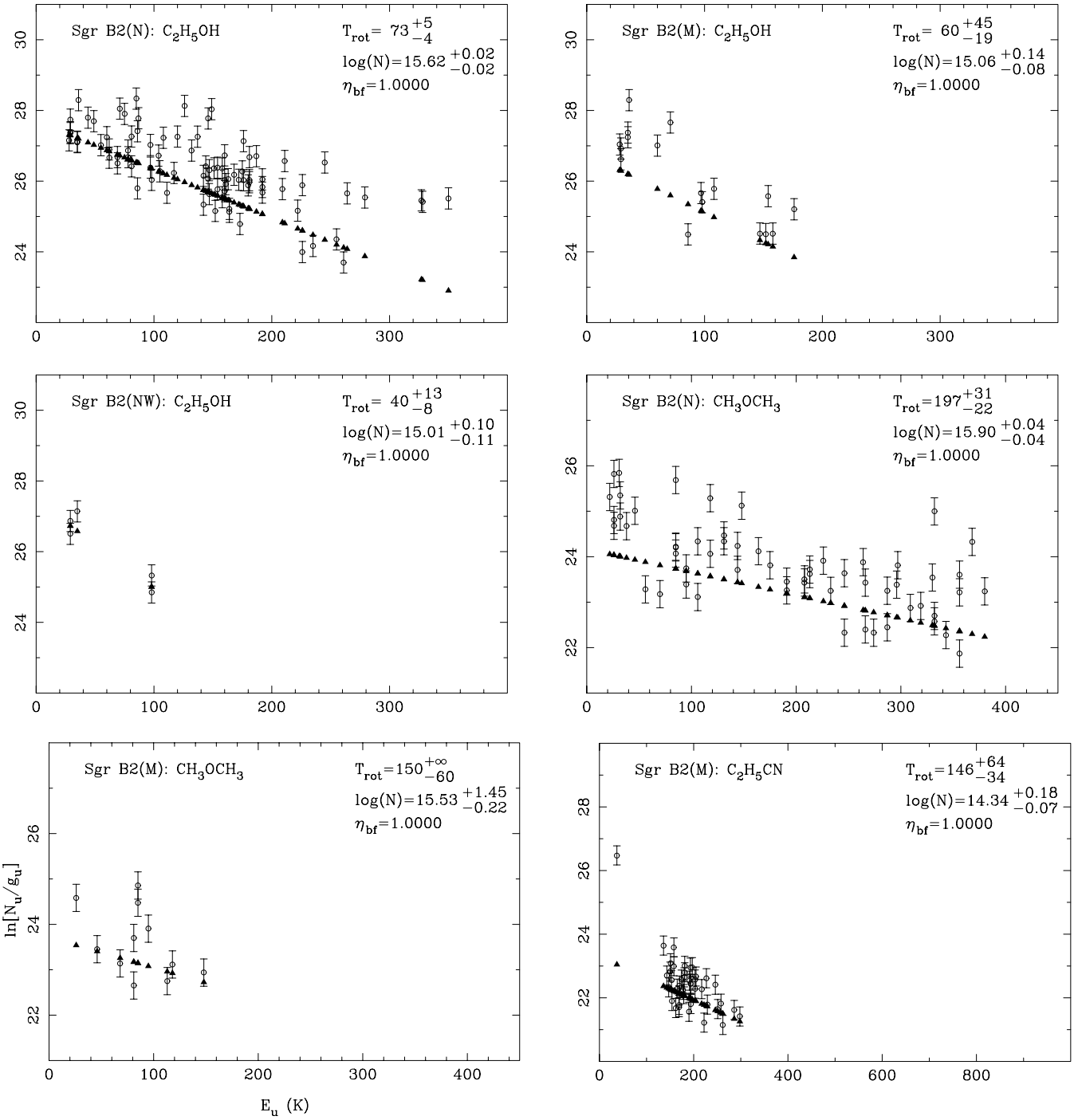

FIG. 2.—*Continued*

In the NW position no $^2\Pi_{3/2}$ lines were detected and a rotation temperature of 20 K was therefore assumed, yielding a column density of 6.3×10^{13} cm^{-2}.

No $N^{34}S$ lines could be identified toward any of the sources, although in N the strongest expected lines at 249.06 and 249.45 GHz could be contributing to the strong line features attributed to CH_3OCHO, C_3H_2, and CH_3OH.

4.7. SO

Sulphur monoxide (SO) was detected in all three observed positions. The SO data in the N and M positions give well-defined χ^2_ν minima for beam-filling factors of 0.035 (4″.4) and 0.06 (5″.8), respectively, by virtue of the detection of the $\Delta J = -1$ and $\Delta J = 0$ transitions, which have 2 orders of magnitude lower A-coefficients than the $\Delta J = +1$ transitions. The resulting rotation temperatures and column densities are 122 K and 3.5×10^{17} cm^{-2} in N, and 135 K and 6.2×10^{17} cm^{-2} in M. The peak optical depths resulting from these models, which occur in the $7_6 \rightarrow 6_5$ line, are 9 and 13, respectively. The fit to the observed line intensities is excellent except for the $2_3 \rightarrow 3_2$ line, which is somewhat too strong compared to the model in M, possibly because of a blend with either C_2H_5OH or C_2H_5CN or both. In NW we derive a rotation temperature of 16 K and a beam-averaged column density of 6.6×10^{14} cm^{-2}.

Lines from ^{34}SO were detected in both N and M. Using the rotation temperatures and beam-filling factors found for the main isotopomer we obtain column densities of

TABLE 1

RESULTS

SPECIES	Sgr B2(N) T_{rot} (K)	Sgr B2(N) N (cm^{-2})	Sgr B2(N) η_{bf}	Sgr B2(M) T_{rot} (K)	Sgr B2(M) N (cm^{-2})	Sgr B2(M) η_{bf}	Sgr B2(NW) T_{rot} (K)	Sgr B2(NW) N (cm^{-2})
$C^{17}O$	50	4.7(16)	...	50	6.0(16)	...	20	9.5(15)
$C^{18}O$	50	1.3(17)[a]	...	50	2.0(17)[a]	...	20	4.1(16)
CS	...	...	...	...	...	...	20	4.4(14)[a]
$C^{34}S$	50	1.9(14)[a]	...	50	2.1(14)[a]	...	20	4.3(13)[a]
^{13}CS	50	2.0(14)[a]	...	50	2.1(14)[a]	...	...	...
$C^{33}S$	50	3.4(13)	...	50	6.4(13)	...	...	...
$^{13}C^{34}S$	50	4.2(13)	...	50	3.5(13)	...	20	7.6(12)
SiO	50	6.8(13)[a]	...	50	9.6(13)[b]	...	20	2.0(13)
^{29}SiO	...	...	...	50	8.9(12)	...	...	...
^{30}SiO	...	...	...	50	4.5(12)	...	...	...
NO	76^{+17}_{-12}	$2.9^{+0.6}_{-0.6}(18)$	$2.6^{+6.4}_{-1.0}(-2)$	62^{+13}_{-10}	$3.1^{+0.9}_{-0.7}(18)$	$1.9^{+2.4}_{-0.8}(-2)$	20	$1.0^{+0.2}_{-0.3}(16)$
NS	76^{+13}_{-10}	$2.7^{+1.4}_{-1.1}(17)$	$2.0^{+0.7}_{-0.6}(-2)$	133^{+38}_{-29}	$4.5^{+1.2}_{-1.2}(14)$	...	20	6.3(13)
SO	122^{+29}_{-27}	$3.5^{+1.7}_{-1.7}(17)$	$3.5^{+0.8}_{-0.9}(-2)$	135^{+29}_{-28}	$6.2^{+2.2}_{-1.8}(17)$	$6.0^{+1.6}_{-1.3}(-2)$	16^{+18}_{-6}	$6.6^{+15}_{-4.1}(14)$
^{34}SO	122	$1.5^{+0.5}_{-0.4}(16)$	3.5(−2)	135	$2.7^{+1.0}_{-0.8}(16)$	6.0(−2)	...	...
^{33}SO	...	...	...	135	$5.8^{+1.5}_{-1.6}(15)$	6.0(−2)	...	...
$S^{18}O$	...	...	...	135	$5.2^{+1.8}_{-1.7}(15)$	6.0(−2)	...	...
SO^+	...	...	...	50	1.9(14)	...	...	
HDO	50	1.1(15)	...	50	6.9(14)	...	...	...
C_2H	50	5.4(14)	...	50	1.1(15)	...	20	4.8(14)
$H^{13}CN$	...	...	...	...	...	...	20	1.1(13)[a]
$HC^{15}N$	50	2.5(13)	...	50	2.0(13)	...	20	3.9(12)
$HN^{13}C$	50	1.8(13)	...	50	2.6(13)	...	20	8.7(12)
$H^{13}CO^+$	50	1.1(13)	...	50	5.4(13)	...	20	9.3(12)
$HC^{18}O^+$	50	5.0(12)	...	50	1.4(13)	...	...	
$HC^{17}O^+$	...	...	...	50	2.1(12)	...	...	
N_2O	50	5.1(15)	...	50	3.3(15)	...	...	
HCS^+	50	8.3(13)	...	50	6.9(13)	...	20	2.7(13)
OCS	50	$6.6^{+1.3}_{-1.6}(15)$[a]	...	50	$5.1^{+1.2}_{-1.1}(15)$[a]	...	20	$1.3^{+0.4}_{-0.4}(16)$
$OC^{34}S$	50	$1.0^{+0.3}_{-0.2}(15)$	...	50	$5.2^{+1.1}_{-1.3}(14)$	...	...	...
^{18}OCS	50	$8.3^{+2.2}_{-2.0}(14)$	...	...	...	...	...	...
$O^{13}CS$	50	2.1(15)	...	50	1.1(15)	...	...	
SO_2	133^{+18}_{-14}	$7.9^{+1.6}_{-1.3}(17)$	$1.3^{+0.3}_{-0.2}(-2)$	183^{+11}_{-11}	$5.0^{+1.0}_{-0.7}(18)$	$1.6^{+0.3}_{-0.2}(-2)$	50^{+126}_{-18}	$2.2^{+2.9}_{-0.5}(14)$
$^{34}SO_2$	133	$1.0^{+0.2}_{-0.2}(17)$	1.3(−2)	183	$2.8^{+0.3}_{-0.2}(17)$	1.6(−2)	...	...
$^{33}SO_2$	...	...	...	183	$4.9^{+1.0}_{-1.0}(16)$	1.6(−2)	...	...
$SO^{18}O$	...	...	...	183	$8.9^{+1.1}_{-1.3}(16)$	1.6(−2)	...	...
$HCNH^+$	...	...	...	...	...	...	20	2.5(14)
H_2CO	50	1.5(15)[a]	...	50	2.6(15)[a]	...	20	2.4(15)[a]
HDCO	50	4.5(13)	...	...	...	...	...	...
$H^{13}{}_2CO$	50	1.2(14)	...	50	7.2(13)	...	...	...
HNCO	212^{+46}_{-34}	$1.7^{+0.3}_{-0.3}(15)$	...	246^{+70}_{-50}	$1.7^{+0.3}_{-0.3}(15)$	...	18^{+6}_{-3}	$1.9^{+2.9}_{-1.2}(15)$
$HOCO^+$	86^{+35}_{-22}	$8.9^{+0.2}_{-0.2}(13)$	...	50	3.3(13)	...	20	6.3(13)
H_2CS	168^{+102}_{-54}	$4.8^{+4.5}_{-1.6}(17)$	$1.4^{+1.1}_{-0.4}(-2)$	69^{+30}_{-18}	$7.6^{+1.5}_{-1.4}(14)$	...	54^{+102}_{-22}	$1.8^{+1.5}_{-0.4}(14)$
CH_2NH	210^{+400}_{-80}	$3.3^{+6.5}_{-1.0}(17)$	$1.4^{+6.5}_{-0.6}(-2)$	44^{+53}_{-15}	$4.1^{+1.8}_{-0.8}(14)$	...	26^{+19}_{-8}	$8.9^{+4.0}_{-3.0}(13)$
c-C_3H_2	13^{+6}_{-4}	$9.1^{+9.1}_{-4.4}(13)$	...	16^{+5}_{-3}	$9.3^{+3.0}_{-2.6}(13)$	...	12^{+6}_{-3}	$3.9^{+3.7}_{-2.0}(13)$
CH_2CN	500	$9.3^{+1.6}_{-1.6}(13)$	...	...	...	...	...	...
CH_2CO	120^{+68}_{-34}	$7.4^{+2.6}_{-1.5}(14)$	...	134^{+114}_{-44}	$5.0^{+3.3}_{-1.2}(14)$	...	...	...
NH_2CN	$500^{+\infty}_{-340}$	$2.3^{+1.5}_{-1.9}(14)$	...	68^{+31}_{-19}	$3.0^{+0.8}_{-0.8}(13)$	...	...	...
HCOOH	74^{+82}_{-30}	$4.2^{+2.0}_{-1.0}(14)$	...	...	...	...	...	...
HC_3N	121^{+56}_{-29}	$8.5^{+2.0}_{-1.3}(16)$	2.7(−2)[c,d]	273^{+45}_{-34}	$4.1^{+0.5}_{-0.4}(16)$	1.3(−2)[c]	20	$1.2^{+0.4}_{-0.4}(15)$
$HCC^{13}CN$	121	$9.8^{+2.5}_{-2.4}(15)$	2.7(−2)[c,d]	273	$5.8^{+1.1}_{-0.9}(15)$	1.3(−2)[c]	...	...
$HC^{13}CCN$	121	$1.6^{+0.4}_{-0.4}(16)$	2.7(−2)[c,d]	273	$4.2^{+0.6}_{-0.8}(15)$	1.3(−2)[c]	...	...
$H^{13}CCCN$	121	$1.1^{+0.3}_{-0.3}(16)$	2.7(−2)[c,d]	276	$6.3^{+1.6}_{-1.2}(15)$	1.3(−2)[c]	...	...
CH_3OH (halo)	45	1.0(16)	...	40	1.0(16)	...	16^{+4}_{-2}	$7.6^{+3.0}_{-3.4}(15)$
CH_3OH (core)	238	5.0(18)	8.0(−3)	150	7.9(18)	2.0(−3)	...	...
$^{13}CH_3OH$ (halo)	45	7.9(14)	...	40	$5.1^{+0.9}_{-1.0}(14)$	...	...	...
$^{13}CH_3OH$ (core)	238	1.0(18)	8.0(−3)	...	...	...	...	...
CH_3CN	400^{+104}_{-86}	$6.3^{+2.2}_{-1.3}(17)$	$1.4^{+1.2}_{-0.3}(-2)$	304^{+128}_{-84}	$3.1^{+1.8}_{-0.7}(17)$	$5.0^{+5.0}_{-2.0}(-3)$	46^{+25}_{-12}	$2.6^{+1.1}_{-0.7}(13)$
$^{13}CH_3CN$	400	$7.2^{+1.1}_{-1.0}(16)$	1.4(−2)	304	$2.5^{+0.5}_{-0.5}(16)$	5.0(−3)	...	...
$CH^{13}{}_3CN$	400	$1.1^{+0.2}_{-0.1}(17)$	1.4(−2)	...	...	...	...	...
NH_2CHO (a-type)	175^{+53}_{-38}	$5.6^{+1.5}_{-1.1}(14)$	...	145^{+62}_{-39}	$2.4^{+0.8}_{-0.5}(14)$	...	...	...
NH_2CHO (b-type)	302^{+126}_{-75}	$9.3^{+3.9}_{-2.4}(15)$	...	...	...	...	...	...
CH_3SH	35^{+17}_{-9}	$1.1^{+0.4}_{-0.3}(15)$	...	41^{+27}_{-12}	$7.8^{+2.5}_{-1.5}(14)$	...	...	...

TABLE 1—*Continued*

Species	Sgr B2(N) T_{rot} (K)	Sgr B2(N) N (cm^{-2})	Sgr B2(N) η_{bf}	Sgr B2(M) T_{rot} (K)	Sgr B2(M) N (cm^{-2})	Sgr B2(M) η_{bf}	Sgr B2(NW) T_{rot} (K)	Sgr B2(NW) N (cm^{-2})
CH_3NH_2	230^{+74}_{-46}	$1.5^{+0.4}_{-0.3}(19)$	$2.2^{+0.8}_{-4.0}(-3)$	...	...	...	...	...
CH_3C_2H	214^{+100}_{-58}	$1.3^{+0.4}_{-0.2}(16)$	...	87^{+18}_{-13}	$7.8^{+0.9}_{-1.0}(15)$	...	120^{+930}_{-60}	$1.4^{+12.4}_{-0.3}(15)$
CH_3CHO (*a*-type)	59^{+22}_{-13}[e]	$4.4^{+0.6}_{-0.5}(14)$[e]	...	47^{+17}_{-10}	$2.7^{+0.5}_{-0.3}(14)$	...	...	...
CH_3CHO (*b*-type)	520^{+1040}_{-220}	$3.2^{+14}_{-1.7}(16)$	...	...	...	...	...	...
c-C_2H_4O	18^{+3}_{-3}[f]	$3.3^{+0.9}_{-0.9}(14)$[f]	...	...	...	...	...	...
C_2H_3CN (core)	440^{+190}_{-90}[g]	$5.1^{+7.2}_{-2.5}(18)$[g]	$1.0^{+0.5}_{-0.3}(-3)$[g]	350^{+510}_{-140}	$4.2^{+38}_{-2.2}(14)$	...	...	...
CH_3OCHO (*a*-type)	200	$5.6^{+0.3}_{-0.1}(15)$	...	$240^{+\infty}_{-160}$	$1.6^{+24}_{-0.7}(15)$	...	...	...
CH_3OCHO (*b*-type)	500	$4.0^{+0.3}_{-0.4}(16)$	...	...	...	...	...	...
C_2H_5OH	73^{+5}_{-4}	$4.2^{+0.2}_{-0.2}(15)$	...	60^{+45}_{-19}	$1.1^{+0.4}_{-0.2}(15)$	...	40^{+13}_{-8}	$1.0^{+0.3}_{-0.2}(15)$
CH_3OCH_3	197^{+31}_{-22}	$7.9^{+0.8}_{-0.7}(15)$	...	$150^{+\infty}_{-60}$	$3.4^{+92}_{-1.3}(15)$	...	...	...
C_2H_5CN (*a*-type)	175^{+25}_{-20}	$1.6^{+0.2}_{-0.1}(15)$	...	146^{+64}_{-34}	$2.2^{+1.1}_{-0.3}(14)$	...	...	...
C_2H_5CN (*b*-type)	210^{+30}_{-30}	$1.5^{+0.4}_{-0.3}(16)$	...	...	...	...	...	...

NOTE.—(1) The source coordinates are (1950.0): Sgr B2(N): $17^h44^m10^s.1$, $-28°21'17''.0$; Sgr B2(M): $17^h44^m10^s.4$, $-28°22'03''.0$; Sgr B2(NW): $17^h44^m06^s.6$, $-28°21'20''.0$. (2) The uncertainties given are 1 σ. The uncertainties stated for the rotation temperatures and column densities do not include uncertainties due to the beam-filling factors.

[a] Probably underestimated owing to saturation.
[b] Probably underestimated owing to self-absorption.
[c] Based on source sizes by Lis et al. 1993.
[d] For HC_3N a vibrational temperature of 425 K was used in Sgr B2(N).
[e] Excluding all torsionally excited lines.
[f] From Dickens et al. 1997.
[g] From Nummelin & Bergman 1999.

1.5×10^{16} cm^{-2} and 2.7×10^{16} cm^{-2}, respectively. The $^{32}SO/^{34}SO$ column density ratios become 23 in both N and M. This is in agreement with the $^{32}S/^{34}S$ abundance ratio quoted by Wilson & Rood (1994) and confirms that the optical depth estimates and, hence, the small inferred source sizes are realistic. Toward M ^{33}SO and $S^{18}O$ were also detected, yielding column densities of 5.8×10^{15} cm^{-2} and 5.2×10^{15} cm^{-2}, respectively, again assuming rotation temperatures and beam-filling factors equal to those found for SO. The isotopomeric column density ratios become $^{32}SO/^{33}SO = 107$ and $S^{16}O/S^{18}O = 120$.

TABLE 2

ISOTOPOMERIC COLUMN DENSITY RATIOS

Ratio	Sgr B2(N)	Sgr B2(M)	Sgr B2(NW)
$C^{18}O/C^{17}O$	2.8 ± 1.2	3.3 ± 1.4	4.3 ± 1.8
$C^{34}S/^{13}C^{34}S$	4.5 ± 1.9	6.0 ± 2.5	5.7 ± 2.4
$^{13}CS/^{13}C^{34}S$	4.8 ± 2.0	6.0 ± 2.5	...
$C^{34}S/C^{33}S$	5.6 ± 2.3	3.3 ± 1.4	...
$^{29}SiO/^{30}SiO$	...	2.0 ± 0.8	...
$SO/^{34}SO$	23^{+13}_{-14}[a]	23^{+11}_{-11}[a]	...
$^{34}SO/^{33}SO$	...	$4.7^{+2.1}_{-1.8}$[a]	...
$SO/S^{18}O$	...	120^{+58}_{-54}[a]	...
$HC^{18}O^+/HC^{17}O^+$	...	6.6 ± 2.8	...
$H^{13}CO^+/HC^{18}O^+$	2.2 ± 0.9	3.9 ± 1.6	...
$OCS/OC^{34}S$	$6.6^{+1.9}_{-2.5}$	$9.8^{+3.4}_{-3.0}$	...
$OCS/O^{13}CS$	$3.1^{+1.1}_{-1.2}$	$4.6^{+1.7}_{-1.7}$	...
$SO_2/^{34}SO_2$	$7.9^{+2.2}_{-2.0}$[a]	$18^{+3.5}_{-3.1}$[a]	...
$^{34}SO_2/^{33}SO_2$	...	$5.7^{+1.4}_{-1.4}$[a]	...
$SO_2/SO^{18}O$	...	56^{+13}_{-11}[a]	...
$H_2CO/HDCO$	33 ± 14	...	...
$HC_3N/HCC^{13}CN$	$8.7^{+3.3}_{-2.4}$[a]	7.1 ± 1.7[a]	...
$HC_3N/HC^{13}CCN$	$5.3^{+2.1}_{-1.4}$[a]	9.8 ± 2.3[a]	...
$HC_3N/H^{13}CCCN$	$7.7^{+3.1}_{-2.2}$[a]	6.5 ± 1.6[a]	...
$CH_3OH/^{13}CH_3OH$	13 ± 5.0[b]	20 ± 8.0[b]	...
$CH_3CN/^{13}CH_3CN$	$8.8^{+3.1}_{-2.1}$[a]	$12^{+8.0}_{-4.0}$[a]	...
$CH_3CN/CH^{13}{}_3CN$	$5.7^{+2.1}_{-1.6}$[a]	...	...

NOTE.—Unless noted the tabulated ratios are not corrected for optical depths. Canonical isotopic ratios in the Galactic center molecular clouds are $^{12}C/^{13}C = 20$; $^{32}S/^{34}S = 22$; $^{29}Si/^{30}Si = 1.5$; $^{16}O/^{18}O = 250$; $^{14}N/^{15}N \geq 600$ (Wilson & Rood 1994); $^{18}O/^{17}O = 3.6$ (Penzias 1981).

[a] This ratio is based on a model with a small beam-filling factor, in which optical depth effects have been accounted for.
[b] Values given refer to the halo (extended) component.

4.8. SO^+

The SO^+ ion was detected toward the M position through the *e* and *f* components of the $J = 11/2 \rightarrow 9/2$ transition (with $E_u = 39$ K). At both frequencies there is emission in N as well, and it is possible that SO^+ may contribute a fraction of the emission detected here, but these lines are essentially lost under the strong lines from C_2H_5CN and OCS, respectively. Also in M the SO^+ transitions are probably somewhat blended with these species. The resulting beam-averaged column density in M is 1.9×10^{14} cm^{-2}.

4.9. HDO

Singly deuterated water vapor, HDO, was detected through its $3_{1,2} \rightarrow 2_{2,1}$ (*b*-type) and $2_{1,1} \rightarrow 2_{1,2}$ (*a*-type) transitions in N and M, although the former line suffers from poor S/N ratio in the N position. The column densities resulting from the $2_{1,1} \rightarrow 2_{1,2}$ line intensities are 1.1×10^{15} cm^{-2} and 6.9×10^{14} cm^{-2} toward N and M, respectively.

4.10. C_2H

The ethynyl radical, C_2H, was detected in its $\Delta J = +1$ components in the $N = 3 \rightarrow 2$ rotational transition toward all three positions; in M also the weaker $\Delta J = 0$ component was seen.

In N the emission from the $J = 7/2 \rightarrow 5/2$ and $J = 5/2 \rightarrow 3/2$ lines covers 40 to 85 km s^{-1} in velocity, and the lines are double-peaked (peaks at 58 and 74 km s^{-1}) with a dip at 65 km s^{-1}. This is more pronounced in the $J = 7/2 \rightarrow 5/2$ component than in the $J = 5/2 \rightarrow 3/2$. In M the

TABLE 3

MOLECULAR ABUNDANCES RELATIVE TO H_2

SPECIES	$X(x) = N(x)/N(H_2)$ Sgr B2(N)	Sgr B2(M)	Sgr B2(NW)
$C^{17}O$	$2(-8)$	$4(-8)$	$2(-8)$
$C^{18}O$	$4(-8)$[a]	$1(-7)$[a]	$7(-8)$
$C^{34}S$	$6(-11)$[a]	$1(-10)$[a]	$7(-11)$[a]
^{13}CS	$7(-11)$[a]	$1(-10)$[a]	...
$C^{33}S$	$1(-11)$	$4(-11)$	...
$^{13}C^{34}S$	$1(-11)$	$2(-11)$	$1(-11)$
SiO	$2(-11)$[a]	$6(-11)$	$3(-11)$
^{29}SiO	...	$5(-12)$	...
^{30}SiO	...	$3(-12)$	...
NO	$2(-7)$[b]	$3(-7)$[b]	$2(-8)$
NS	$1(-8)$[b]	$3(-10)$	$1(-10)$
SO	$2(-8)$[b]	$1(-7)$[b]	$1(-9)$
^{34}SO	$1(-9)$[b]	$4(-9)$[b]	...
^{33}SO	...	$9(-10)$[b]	...
$S^{18}O$	...	$8(-10)$[b]	...
SO^+	...	$1(-10)$	...
HDO	$4(-10)$	$4(-10)$	...
C_2H	$2(-10)$	$6(-10)$	$8(-10)$
$H^{13}CN$	...	...	$2(-11)$
$HC^{15}N$	$8(-12)$	$1(-11)$	$7(-12)$
$HN^{13}C$	$6(-12)$	$2(-11)$	$1(-11)$
$H^{13}CO^+$	$4(-12)$	$3(-11)$	$2(-11)$
$HC^{18}O^+$	$2(-12)$	$8(-12)$	...
$HC^{17}O^+$	...	$1(-12)$	...
N_2O	$2(-9)$	$2(-9)$	...
HCS^+	$3(-11)$	$4(-11)$	$5(-11)$
OCS	$2(-9)$[a]	$3(-9)$[a]	$2(-8)$
$OC^{34}S$	$3(-10)$	$3(-10)$	...
$O^{13}CS$	$7(-10)$	$6(-10)$	...
SO_2	$3(-8)$[b]	$4(-7)$[b]	$4(-10)$
$^{34}SO_2$	$4(-9)$[b]	$2(-8)$[b]	...
$^{33}SO_2$	...	$4(-9)$[b]	...
$SO^{18}O$	...	$7(-9)$[b]	...
$HCNH^+$	...	...	$4(-10)$
H_2CO	$5(-10)$[a]	$2(-9)$[a]	$4(-9)$[a]
HDCO	$2(-11)$	...	...
$H_2^{13}CO$	$4(-11)$	$4(-11)$	...
HNCO	$6(-10)$	$1(-9)$	$3(-9)$
$HOCO^+$	$3(-11)$	$2(-11)$	$1(-10)$
H_2CS	$2(-8)$[b]	$4(-10)$	$3(-10)$
CH_2NH	$1(-8)$[b]	$2(-10)$	$1(-10)$
c-C_3H_2	$3(-11)$	$5(-11)$	$7(-11)$
CH_2CN	$3(-11)$	...	...
CH_2CO	$2(-10)$	$3(-10)$	...
NH_2CN	$9(-11)$	$2(-11)$	...
HCOOH	$1(-10)$	...	...
HC_3N	$5(-9)$[b]	$3(-9)$[b]	$2(-9)$
$HCC^{13}CN$	$6(-10)$[b]	$4(-10)$[b]	...
$HC^{13}CCN$	$1(-9)$[b]	$3(-10)$[b]	...
$H^{13}CCCN$	$7(-10)$[b]	$5(-10)$[b]	...
CH_3OH (halo)	$3(-9)$	$6(-9)$	$1(-8)$
CH_3OH (core)	$2(-7)$[b]	$2(-7)$[b]	...
$^{13}CH_3OH$ (halo)	$3(-10)$	$3(-10)$	...
$^{13}CH_3OH$ (core)	$3(-8)$[b]	...	...
CH_3CN	$3(-8)$[b]	$2(-8)$[b]	$4(-11)$
$^{13}CH_3CN$	$3(-9)$[b]	$1(-9)$[b]	...
$CH^{13}{}_3CN$	$5(-9)$[b]	...	...
NH_2CHO (a-type)	$2(-10)$	$1(-10)$	...
CH_3SH	$4(-10)$	$5(-10)$	...
CH_3NH_2	$3(-7)$[b]	...	...
CH_3C_2H	$4(-9)$	$5(-9)$	$2(-9)$
CH_3CHO (a-type)	$2(-10)$	$2(-10)$	...
c-C_2H_4O	$1(-10)$	...	...
C_2H_3CN (halo)	$4(-10)$	...	...
C_2H_3CN (core)	$6(-8)$[b]	$2(-10)$	...
CH_3OCHO (a-type)	$1(-9)$	$9(-10)$	...
C_2H_5OH	$1(-9)$	$6(-10)$	$2(-9)$
CH_3OCH_3	$3(-9)$	$2(-9)$	...
C_2H_5CN (a-type)	$6(-10)$	$1(-10)$	...

NOTE.—For source sizes significantly smaller than 23″ the beam-averaged abundances tabulated will be underestimates (See § 5.1).

[a] Should be considered a lower limit due to saturation effects (see § 4).

[b] Using an estimated source size, see Table 1 and the discussion in § 5.1.

emission features extend over wider ranges of velocities, $30 \rightarrow 110$ km s^{-1}. The peak of the emission falls at 55 km s^{-1}, which is somewhat low compared to the emission velocities of other species, and may indicate absorption around 60–70 km s^{-1}. In NW the emission is again double-peaked with one velocity component at 59 km s^{-1} and the other one at 77 km s^{-1}.

The integrated intensities were calculated across the full velocity width of the lines. The column densities become, assuming a rotation temperature of 50 K in N and M and 20 K in NW, 5.4×10^{14} cm^{-2}, 1.1×10^{15} cm^{-2}, and 4.8×10^{14} cm^{-2} in N, M, and NW, respectively. However, it should be noted that the lines may suffer from self-absorption and that our assumption of optically thin emission therefore may be a poor approximation. Moreover, if the C_2H emission mainly originates in the outer cloud envelope, as indicated by the wide range of emission velocities, the actual rotation temperature may be substantially lower than 50 K.

4.11. HCN

The main isotopomer of hydrogen cyanide, HCN, has no lines within the observed spectral band; however, the $J = 3 \rightarrow 2$ transitions of the ^{13}C and ^{15}N isotopomers were detected. The $H^{13}CN$ line is severely self-absorbed in N and M and cannot be analyzed by assuming uniform excitation along the line of sight. In NW we deduce a column density of 1.1×10^{13} cm^{-2}, assuming 20 K. The emission in this position peaks at low velocities, 53 km s^{-1}, which may indicate that self-absorption occurs at higher velocities, similar to what is clearly seen in N and M. The $HC^{15}N$ transition does not seem to suffer from any absorption such as that seen in $H^{13}CN$, and the column densities become 2.5×10^{13} cm^{-2} and 2.0×10^{13} cm^{-2} in N and M, respectively. In M the irregular line profile seems to be due to a velocity component near 50 km s^{-1} besides the main component around 62 km s^{-1}. In NW the emission peaks around 58 km s^{-1} and a column density of 3.9×10^{12} cm^{-2} is deduced. DCN has no transition in the frequency band covered.

4.12. HNC

Hydrogen isocyanide, HNC, was detected through the $J = 3 \rightarrow 2$ transition of $HN^{13}C$ in all three positions. The velocity structure of this line is rather complex. In N the peak emission occurs at 59 km s^{-1}, with a broad shoulder on the low-velocity side extending down to about 30 km s^{-1}, although the $HN^{13}C$ wing emission is most likely blended with emission from C_2H_5OH in its gauche-conformation. The feature at 70 km s^{-1} has been assigned to C_2H_3CN. In M the main velocity component appears at 55 km s^{-1}, which is somewhat low. Furthermore, there is either an absorption dip at 63 km s^{-1}, which may indicate that the line is slightly self-absorbed, or emission from another cloud component at 68 km s^{-1}. There is also a broad line-wing extending to 90 km s^{-1}. In NW the main emission component is located at 56 km s^{-1} and there are intermixed weaker emission components extending to about 80 km s^{-1}.

The $HN^{13}C$ column densities become 1.8×10^{13} cm^{-2}, 2.6×10^{13} cm^{-2}, and 8.7×10^{12} cm^{-2} in N, M, and NW, respectively. These values could actually be lower limits in case $HN^{13}C$ suffers from self-absorption in any of the sources. The DNC $J = 3 \rightarrow 2$ line was not detected in any of

the sources. For $T_{mb} \leq 0.2$ K, we estimate the upper limits on the column density of DNC to be 3×10^{12} cm^{-2} in N and NW, and 4×10^{12} cm^{-2} in M. Assuming $^{12}C/^{13}C = 20$ (Wilson & Rood 1994), we find lower limits on the HNC/DNC abundance ratio of 120 (N), 130 (M), and 58 (NW).

The $H^{13}CN/HN^{13}C$ column density ratio in NW becomes 1.3. By assuming a $^{14}N/^{15}N$ ratio of 600 and a $^{12}C/^{13}C$ ratio of 20, we can make a crude estimate of the HCN/HNC abundance ratio in all three positions using the $HC^{15}N$ and $HN^{13}C$ column densities. The resulting HCN/HNC ratios are 42, 23, and 13 in N, M, and NW, respectively, indicating high cloud temperatures (Goldsmith et al. 1986; Schilke et al. 1992). Thus, to account for the small $H^{13}CN/HN^{13}C$ column density ratio in NW the $H^{13}CN$ line must be optically thick ($\tau \sim 10$).

4.13. HCO^+

No transition of the main isotopomer of the formyl ion, HCO^+, falls within the frequency band studied, but the $H^{13}CO^+$, $HC^{18}O^+$, and $HC^{17}O^+$ $J = 3 \rightarrow 2$ lines were detected. In M the $H^{13}CO^+$ emission peaks at 54 km s^{-1} and extends to about 85 km s^{-1}, although the wing emission could be slightly blended with CH_3OCHO. In N the main component occurs at 58 km s^{-1}, and the component at lower (around 45 km s^{-1}) velocities is interpreted as being mainly due to C_2H_5OH. The $H^{13}CO^+$ column densities become 1.1×10^{13} cm^{-2} in N, and 5.4×10^{13} cm^{-2} in M. Toward NW the line profile is slightly asymmetric with a high-velocity wing as seen in M, and with the peak emission at 59 km s^{-1}. The column density in NW is 9.3×10^{12} cm^{-2}. The $HC^{18}O^+$ line is centered at 65 km s^{-1} in N and at 62 km s^{-1} in M, but is blended with a number of U-lines in N. The column densities for N and M are 5.0×10^{12} cm^{-2} and 1.4×10^{13} cm^{-2}, respectively. The low $H^{13}CO^+/HC^{18}O^+$ column density ratios deduced in N and M indicate optically thick emission in $H^{13}CO^+$. $HC^{17}O^+$ was detected only in M, yielding a column density[4] of 2.1×10^{12} cm^{-2}, and a $HC^{18}O^+/HC^{17}O^+$ column density ratio of 6.6 ± 2.8.

4.14. N_2O

Nitrous oxide, N_2O, is detected through its $J = 9 \rightarrow 8$ transition in N and M. The column densities become 5.1×10^{15} cm^{-2} and 3.3×10^{15} cm^{-2} in N and M, respectively. However, in N the S/N ratio is poor and in M the line is weak, which makes the identification of this transition uncertain in both positions.

4.15. HCS^+

The thioformyl ion, HCS^+, was detected through its $J = 6 \rightarrow 5$ line in all three positions. The column densities become 8.3×10^{13} cm^{-2}, 6.9×10^{13} cm^{-2}, and 2.7×10^{13} cm^{-2}, respectively.

4.16. OCS

Carbonyl sulfide, OCS, was detected in all three positions. Four rotational transitions are available in the observed band, but the energy separation between the rotational levels is rather small, and the range of upper-state energies covered is therefore too narrow to allow a reliable estimate of the rotation temperature. A rotation temperature of 50 K in N and M and 20 K in NW was assumed in order to determine beam-averaged column densities. The resulting OCS column densities are 6.6×10^{15} cm^{-2}, 5.1×10^{15} cm^{-2}, and 1.3×10^{16} cm^{-2} in N, M, and NW, respectively. The $OC^{34}S$ isotopomer was detected in N and M. Using the same assumption on rotation temperature as for the main isotopomer the resulting $OCS/OC^{34}S$ column density ratio is 7 in N and 10 in M, which may indicate somewhat optically thick OCS emission in both cores. The $O^{13}CS$ isotopomer was detected only through two transitions in N and one transition in M and, under the same assumptions as above, the resulting $OCS/O^{13}CS$ column density ratio is 3 in N and 5 in M, again indicating optically thick emission in both positions. In N ^{18}OCS seems to be detected through three lines, yielding a $OCS/^{18}OCS$ column density ratio as low as 8. However, this unexpectedly low $OCS/^{18}OCS$ ratio, taken together with the facts that the $21 \rightarrow 20$ and $22 \rightarrow 21$ lines of ^{18}OCS are suspected to be blended with other species and that the $23 \rightarrow 22$ line is overlapping an unidentified line, make the identification of this isotopomer doubtful.

4.17. SO_2

Sulphur dioxide, SO_2, is one of the most interesting molecules detected in the survey. It contributes 20% of the observed line flux from Sgr B2(M) and is the dominant source of line emission from this source, with the exception of CO. It could therefore contribute significantly to the cloud cooling in this frequency regime. SO_2 was also detected in Sgr B2(N) and Sgr B2(NW), although less prominently. In N and M a number of rotational lines in the v_2 vibrational state, at 745 K above the ground state, were detected in addition to the ground state lines.

The best agreement with the data was obtained for small beam-filling factors, 0.013 for N and 0.016 for M, and rotation temperatures of 133 and 183 K for N and M, respectively. The corresponding source sizes are 2.″6 and 2.″9, respectively, assuming Gaussian beam (23″) and source distributions. This is in agreement with recent high angular resolution observations of SO_2 in Sgr B2(M), performed with the Owens Valley Radio Interferometer, which indicate a similarly small source size (Bergman et al. 2000, in preparation). The shape of the minimum in the χ^2_ν-values found for the small beam-filling factor is distinct (see Fig. 1) and relies on the detection of a large number of Q, R, and P-branch transitions (in order of decreasing line strength). The resulting column densities, adopting the above source sizes, become 7.9×10^{17} cm^{-2} and 5.0×10^{18} cm^{-2} for N and M, respectively. The peak optical depths, which occur in the $13_{1,13} \rightarrow 12_{1,12}$ transition, are 14 in M and 5 in N. The lines in the v_2 vibrational state were included together with the ground-state lines in the analysis. In N the adopted model does not successfully reproduce the observed intensities of the v_2 lines, but leads to predictions that are 10–50 times too weak. Excluding the vibrationally excited lines from the analysis does not significantly change either the rotation temperature, the column density, or the best-fitting beam-filling factor. In M the model fits reasonably well also to the v_2 lines, although these lines are more scattered than the ground-state lines. However, if the v_2 lines are included, the best-fit rotation temperature increases from 165 K to 182 K, while the column density increases slightly from

[4] The A coefficient stated for $HC^{17}O^+$ in Table 15 of Paper I is incorrect; the correct value is 9.7×10^{-4}.

4.1×10^{18} cm^{-2} to 5.0×10^{18} cm^{-2}. The excitation of the v_2 state is likely to be affected by 19 μm radiation from hot dust, which may be characterized by a radiation temperature higher than the rotational temperature of 150–200 K.

In M most of the strong SO_2 transitions have asymmetric line profiles. In addition to the main Gaussian line component at the normal emission velocity, 59–60 km s^{-1}, there is usually another component at slightly higher velocity, 62–64 km s^{-1}, which makes these lines somewhat more convex than a Gaussian line profile. Most of the lines with this appearance are estimated to be rather optically thick.

A large number of lines from $^{34}SO_2$ were also detected, primarily in M but also a few ones in N. Keeping the beam-filling and rotation temperature fixed at the values found for the ^{32}S isotopomer yields a column density of 1.0×10^{17} cm^{-2} in N and 2.8×10^{17} cm^{-2} in M. This yields an $SO_2/^{34}SO_2$ column density ratio of 8 ± 2 in N, and 18 ± 3 in M, at least in M in good agreement with the measured cosmic elemental $S/^{34}S$ ratio of 22 (Wilson & Rood 1994). In N the $^{34}SO_2$ column density is uncertain owing to the small number of lines detected. If the rotation temperature instead is kept as a free parameter in M, the best-fitting temperature becomes 140 K, but the column density is almost unchanged, 2.7×10^{17} cm^{-2}. In Sgr B2(M) we also detected a number of lines from $^{33}SO_2$ and $SO^{18}O$. The resulting column densities are, using the rotation temperature and beam-filling factor deduced for the main isotopomer, 4.9×10^{16} cm^{-2} and 8.9×10^{16} cm^{-2}, respectively. The isotopomeric column density ratios become $N(SO_2)/N(^{33}SO_2) = 102$ and $N(SO_2)/N(SO^{18}O) = 56$. Since the two possible placements of the ^{18}O atom in $SO^{18}O$ give indistinguishable molecular configurations the $SO_2/SO^{18}O$ abundance ratio should theoretically be a factor 2 smaller than the $^{16}O/^{18}O$ ratio, assuming no chemical fractionation. Hence, the $^{16}O/^{18}O$ abundance ratio indicated by the $SO_2/SO^{18}O$ column density ratio of 56 is consistent with the deduced $SO/S^{18}O$ ratio of about 120.

4.18. $HCNH^+$

Protonated hydrogen cyanide, $HCNH^+$, is the only molecule in the survey to be detected exclusively in the NW position. The $J = 3 \rightarrow 2$ line has two rather weak velocity components at 59 and 75 km s^{-1}, yielding a total column density of 2.5×10^{14}cm^{-2}. Although no definite identification of $HCNH^+$ could be made in N, there is a line, which has been assigned to CH_2CO and vibrationally excited C_2H_3CN, near the frequency of $HCNH^+$ ($J = 3 \rightarrow 2$), to which there may be some contribution from $HCNH^+$. However, if this line feature was mainly due to $HCNH^+$, the emission velocity would be somewhat high, 75 km s^{-1}. Conversely, we do not believe that the line feature in NW is due to CH_2CO, since no other, similarly strong lines of this species with the same excitation energies are seen in that position.

4.19. H_2CO

The main isotopomer of formaldehyde, H_2CO, is detected through three transitions in the survey. Of these, the $3_{1,2} \rightarrow 2_{1,1}$ line ($E_u = 33$ from the ortho species cannot be analyzed assuming uniform excitation along the line of sight, since the line profiles in both N and M have deep absorptions superimposed on the emission lines. The two para transitions have higher upper-state energies (68 K), and are apparently less affected by absorption. In N both para lines have peak emission velocity at 60 km s^{-1}, are steep on the high-velocity side, and have a low velocity wing extending to about 30 km s^{-1}. In M the emission peaks at 56 km s^{-1} and exhibits a wing on the high-velocity side, extending to about 100 km s^{-1}. In NW the lines have two equally strong velocity components at 60 and 74 km s^{-1}. Using the unblended $3_{2,1} \rightarrow 2_{2,0}$ para line, the resulting column densities become 1.5×10^{15} cm^{-2} and 2.6×10^{15} cm^{-2} in N and M, respectively. In NW we derive 2.4×10^{15} cm^{-2}. However, considering that the emission velocities in N and M are somewhat low compared to other molecules and also compared to $H_2^{13}CO$ (see below), there is a possibility that there are self-absorptions on the high-velocity sides of the 68 K lines and that the column densities have been underestimated.

The $H_2^{13}CO$ isotopomer was detected through the $3_{1,2} \rightarrow 2_{1,1}$ ortho line toward N and M, although in N the line may be somewhat blended with the $12_{3,10} \rightarrow 11_{2,9}$ line of C_2H_5CN. The emission velocity for the $H_2^{13}CO$ line is around 64 km s^{-1} in N and 60 km s^{-1} in M. The column densities are 1.2×10^{14} cm^{-2} and 7.2×10^{13} cm^{-2}, and the resulting $H_2CO/H_2^{13}CO$ column density ratios become 13 and 36 in N and M, respectively. However, we note that the total (ortho + para) H_2CO and $H_2^{13}CO$ column densities rely on lines from the para and ortho species, respectively, and therefore the estimated $H_2CO/H_2^{13}CO$ column density ratio depends on the assumed (optically thin) ortho/para ratio of 3. In N, HDCO was detected through two lines. Using the $4_{2,3} \rightarrow 3_{2,2}$ line, the HDCO column density becomes 4.5×10^{13} cm^{-2}, yielding a $H_2CO/HDCO$ column density ratio of only 33. By replacing $N(H_2CO)$ with $20 \times N(H_2^{13}CO)$ the ratio becomes 53.

4.20. HNCO

Isocyanic acid, HNCO, was detected toward N, M, and NW primarily through its *a*-type, *R*-branch transitions, but in N and M also through the high-energy *P*-branch, *b*-type $28_{1,28} \rightarrow 29_{0,29}$ and $27_{1,27} \rightarrow 28_{0,28}$ lines. The rotation temperatures are rather high, 212 K in N and 246 K in M, and the beam-averaged column densities are 1.7×10^{15} cm^{-2} in both positions. Only the lowest-lying transition, $10_{0,10} \rightarrow 9_{0,9}$ ($E_u = 58$ K), seems to be excessively strong, by a factor of 5 compared to this model, which may be caused by contribution of emission from an extended, cool envelope. The rotation temperatures and column densities inferred by the lines below 150 K (tracing cool gas) are about 30 K and $\sim 2 \times 10^{15}$ cm^{-2}, respectively, in both N and M. In NW a rotation temperature of 18 K and a column density of 1.9×10^{15} cm^{-2} fits the data well. For most of the lines, the ^{13}C isotopomer is blended with and lost under the main isotopomer lines on the low-velocity side, but, considering the apparently low optical depths in the main isotopomer, their contribution to the integrated intensity of HNCO is probably insignificant.

4.21. $HOCO^+$

Protonated carbon dioxide, $HOCO^+$, was detected in all three positions, but only in N through more than one line. The deduced rotation temperature in N is 86 K and the beam-averaged column density is 8.9×10^{13} cm^{-2}. By assuming a rotation temperature of 50 K in M and 20 K in

NW, column densities of 3.3×10^{13} cm^{-2} and 6.3×10^{13} cm^{-2} were derived, respectively.

4.22. H_2CS

Thioformaldehyde, H_2CS, was detected through lines from both its ortho and para species in all three positions. The standard ratio of 3:1 was assumed for the statistical weights between the ortho and para species. In N the best fit to the data is obtained for a beam-filling factor of 0.014, which is consistent with the source size found for SO_2. In M a beam-filling factor $\eta_{bf} < 1$ does not fit the data significantly better than $\eta_{bf} = 1$ in a statistical sense. Therefore, the column densities and rotation temperatures reported here refer to a beam-filling factor of 0.014 for N, but are beam-averaged quantities for M and NW. The rotation temperatures are 168, 69, and 54 K, and the column densities are 4.8×10^{17} cm^{-2}, 7.6×10^{14} cm^{-2}, and 1.8×10^{14} cm^{-2} in N, M, and NW, respectively. For comparison with the value in the N position, the column density in M for a beam-filling factor of 0.014 (the same as in N) becomes 7.6×10^{16} cm^{-2}. In N the optical depths are about 4 in the best-fit model, which makes it somewhat surprising that none of the $H_2C^{34}S$ lines could be identified. However, because of the lack of molecular distortion constants for this isotopomer (Johnson, Lovas, & Kirchhoff 1972), the predicted rest frequencies may be too inaccurate to allow line identification.

4.23. CH_2NH

Methylenimine, CH_2NH, is the only molecule in the survey which has a ground state transition in the observed band. The $1_{1,1} \rightarrow 0_{0,0}$ line, which has an unresolved hyperfine-splitting ($\sim$2 MHz) due to the quadrupole moment of the nitrogen nucleus, is seen in absorption toward N and M, and, weakly, also toward NW. The absorption lines each have two components: at 64 (main component) and 80 km s^{-1} in N, and at 59 and 68 km s^{-1} (main component) in M. We can calculate the peak optical depth of the $1_{1,1} \rightarrow 0_{0,0}$ absorption line through

$$\tau_0 = \ln\left(\frac{1}{1-R}\right), \tag{9}$$

where

$$R = \frac{T_c - T_{abs}}{T_c}, \tag{10}$$

and where T_{abs} is the observed intensity at the peak of the absorption, and T_c is the observed continuum brightness temperature. The resulting optical depths for the unresolved group of hyperfine components are 2.1 in N and 1.9 in M. The column density of absorbing gas is

$$N = 3.6 \times 10^{12} \frac{Q(T)}{1 - e^{-10.8/T}} \Delta V \tau_0 . \tag{11}$$

Since the absorption occurs in the low-excitation gas in front of the continuum sources the temperature to be used in the equation above should probably be somewhat lower than the 50 K used for the emission lines. Hence, using ΔV equal to 13 km s^{-1} toward N and 17 km s^{-1} toward M, the CH_2NH column densities become, for an assumed temperature of 20 K, 8.0×10^{15} cm^{-2} and 9.4×10^{15} cm^{-2} toward N and M, respectively.

In the N position, the lines detected in emission are best fitted using a beam-filling of 0.014, and the resulting column density is 3.3×10^{17} cm^{-2} for a rotation temperature of 210 K. In M no significant improvement in the fit to the data was obtained for a beam-filling factor less than 1. Here the rotation temperature is significantly lower, 44 K, and the beam-averaged column density becomes 4.2×10^{14} cm^{-2}. In NW the best-fit temperature and column density are 26 K and 8.9×10^{13} cm^{-2}, respectively. Thus, both cool extended CH_2NH and a hot core seems to be present toward N and, possibly, M.

4.24. c-C_3H_2

Cyclopropenylidene, c-C_3H_2, is one of two cyclic molecules identified in the survey. The rotation temperatures in the three positions show little variation and are very low, 13, 16, and 12 K in N, M, and NW, respectively. The beam-averaged column densities are also rather similar, 9.1×10^{13} cm^{-2} in N, 9.3×10^{13} cm^{-2} in M, and 3.9×10^{13} cm^{-2} in NW. The $5_{2,3} \rightarrow 4_{3,2}$ line seems a factor of 3 too strong compared to the model in both N and M, which could be due to a blend with emission from CH_3OCHO and/or $N^{34}S$. Judging from the low rotational temperatures, it is likely that the c-C_3H_2 emission mainly originates from envelope gas of low excitation.

4.25. CH_2CN

The cyanomethyl radical, CH_2CN, was detected in the N position through nine transitions. Despite the fact that only a-type transitions, all with similar A-coefficients, have been detected, the appearance of the rotation diagram is very scattered and no reliable value of the rotation temperature could be obtained from a fit to the data. These problems may be due to peculiar excitation of this molecule, or simply to misidentifications of several lines. In lack of an estimate of the rotation temperature 500 K was assumed, resulting in a column density of 9.3×10^{13} cm^{-2}.

4.26. CH_2CO

Ketene, CH_2CO, was detected in N and M, and the best-fitting rotation temperatures are 120 and 134 K, respectively. The beam-averaged column densities are 7.4×10^{14} cm^{-2} in N and 5.0×10^{14} cm^{-2} in M. The $12_{3,10/9} \rightarrow 11_{3,9/8}$ doublet seems somewhat strong in the rotation diagram for N, which is most likely due to a blend with C_2H_5CN.

4.27. NH_2CN

Cyanamide, NH_2CN, was detected toward N through a-type transitions in the ground state and in the lowest vibrational state, which is the NH_2 inversion at 71 K above the ground state. In M only ground state transitions were detected. It should be noted that in vibrational states with v even (including $v = 0$), the statistical weights are 3 for levels with K_a odd and 1 for levels with K_a even, but the opposite holds for states with v odd. In N the (marginally) best fit is obtained for a small beam-filling factor, $\eta_{bf} = 0.01$, and a low ($\approx$40 K) rotation temperature. However, the improvement of the goodness-of-fit as compared to the best fit using $\eta_{bf} = 1.0$ is less than 1 σ, and thus not statistically significant, although a low rotation temperature is consistent with the result obtained in the M position. Hence, the best-fitting model parameters is considered to be a beam-filling factor

of 1.0, a rotation temperature of 500 K, and a column density of 2.3×10^{14} cm^{-2}, although the rotation temperature is virtually unconstrained upward. It is possible that the vibrationally excited lines are tracing a hot gas component in N, or that the vibrational levels are populated primarily through radiative rotation-inversion transitions around 200 μm. Another alternative is that the vibrationally excited lines may be severely blended or misidentifications.

In M only lines in the ground state were detected and the best-fit rotation temperature is 68 K and the column density is 3.0×10^{13} cm^{-2}.

4.28. HCOOH

Formic acid, HCOOH, was detected only in N. The rotation temperature deduced for this molecule is 74 K, which yields a column density of 4.2×10^{14} cm^{-2}. The fit to the data is rather poor, however.

4.29. HC_3N

Cyanoacetylene, HC_3N, was detected in its ground vibrational state toward all three positions. In addition, rotational lines in the fundamental doubly degenerate CCC (v_7), CCN (v_6), and HCC (v_5) bending modes, and the (nondegenerate) C—C stretch (v_4) were detected in the N and M positions (see Wyrowski, Schilke, & Walmsley 1999). Also the combination mode (v_4, v_5, v_6, v_7) = (0, 0, 1, 1) was detected in N. Table 4 lists a few vibrationally excited HC_3N lines assigned after Paper I went to press. In particular toward the N position the vibrationally excited lines have additional emission components both at low (around 50 km s^{-1}) and high (around 75 km s^{-1}) velocities.

Using the source sizes from Lis et al. (1993), who observed the HC_3N $J = 25 \rightarrow 24$ beam-filling factors equal to 0.027 in N and 0.013 in M. These source sizes are valid for emission from the ground state, but we would expect the vibrationally excited lines to arise in even smaller regions because of the severe excitation requirements.

It seems from the rotation diagram toward the N position as if the rotational temperature within a given vibrational state differs from the temperature that determines the relative population in the different vibrational states (the vibration temperature). One plausible explanation for this is that the HC_3N level populations within a vibrational state are determined primarily by H_2 collisions, while the entire population of a vibrational state is determined by radiative processes in the far-infrared. Although this appearance of the rotation diagram could also be an effect of high optical depths, we have not been able to find an adequate fit for any physically plausible set of column density, source-size, and rotation temperature. In N we therefore used a model in which the optical depths were calculated through (cf. eq. [4])

$$\tau_{ul} = \sqrt{\frac{\ln 2}{16\pi^3}} \frac{c^3 A_{ul} g_u N}{\nu_{ul}^3 Q(T_{\rm rot}, T_{\rm vib}) \Delta V} \times e^{-(E_u - E_{\rm vib})/kT_{\rm rot}} e^{-E_{\rm vib}/T_{\rm vib}} (e^{h\nu_{ul}/kT_{\rm rot}} - 1) , \quad (12)$$

where $E_{\rm vib}$ is the energy difference between the ground state and the vibrational state, and where $Q(T_{\rm rot}, T_{\rm vib})$ is the rotation-vibration partition function. The best fit to data in Sgr B2(N) was obtained using a rotation temperature of 121 K and a vibration temperature of about 425 K, which yield a column density of 8.5×10^{16} cm^{-2}. This is the total column density of HC_3N in the ground state and the five excited vibrational states in which lines were detected. The derived vibrational temperature of 425 K is very similar to the temperature of 440 K found for hot C_2H_3CN (Nummelin & Bergman 1999). In M there is no pronounced difference between the rotational and vibrational temperatures. Hence, the standard model, with a single temperature, was applied in the M position. This model yields a rotation temperature 273 K, and a total column density of 4.1×10^{16} cm^{-2}. In NW only two unblended ground-state transitions were detected, and the beam-averaged column density, assuming a rotation temperature of 20 K, is 1.2×10^{15} cm^{-2}. Given the rotation/vibration temperatures inferred in N and M, we do not expect the population in nondetected vibrational states higher than 1400 K to be significant.

In N and M the three ^{13}C isotope variants of HC_3N were detected in the ground state. Using the rotation temperatures from the main isotopomer, 107 and 273 K, and a vibration temperature of 425 K in N, the $^{12}C/^{13}C$ ratios become 5–9 and 7–10 in N and M, respectively.

4.30. CH_3OH

Methanol, CH_3OH, is detected through a large number of lines in all three positions observed, and is the molecule which contributes most (about 13%) of the total observed spectral-line flux toward Sgr B2(N). In N and M rotational lines were detected in the first ($v_t = 1$) and second ($v_t = 2$) torsionally excited states. The detected transition with lowest energy, the $2_0 \rightarrow 1_{-1}$ of the E species (at 19 K), is seen in a combination of emission and absorption toward N and M. Many of the CH_3OH lines detected toward N and

TABLE 4

SOME ADDITIONAL HC_3N LINE IDENTIFICATIONS

REST FREQUENCY (MHz)	TRANSITION (J_ℓ)	VIBRATIONAL STATE (v_4, v_5, v_6, v_7)	E_u (K)	$A_{\rm ul}$ (s^{-1})	$\int T_{\rm mb}\, dv$ (K km s^{-1}) N	M	NW	REMARKS
219411.6	$24_{0e} \rightarrow 23_{0e}$	(0, 0, 1, 1)	1167	8.35×10^{-4}	11.3	...	...	b $CH^{18}{}_3OH$
219436.7	$24_{0f} \rightarrow 23_{0f}$	(0, 0, 1, 1)	1167	8.35×10^{-4}	8.0	...	...	b NH_2CN
236184.0	$26_{0e} \rightarrow 25_{0e}$	(1, 0, 0, 0)	1393	1.04×10^{-3}	13.5	...	...	prev. U236184
245264.6	$27_{0e} \rightarrow 26_{0e}$	(1, 0, 0, 0)	1405	1.17×10^{-3}	8.3	...	...	prev. U245267
246813.4	$27_{0e} \rightarrow 26_{0e}$	(0, 0, 1, 1)	1201	1.19×10^{-3}	9.4	...	...	prev. U246816
246849.0	$27_{0f} \rightarrow 26_{0f}$	(0, 0, 1, 1)	1201	1.19×10^{-3}	5.4	...	...	prev. U246851
246930.4	$27_{2f} \rightarrow 26_{2f}$	(0, 0, 1, 1)	1201	1.15×10^{-3}	5.1	...	...	b CH_3NH_2/HDCO

M exhibit some velocity structure such as wing emission on both the high- and low-velocity side.

From inspection of the rotation diagrams for CH_3OH, it is clear that there are gradients in the excitation conditions in both Sgr B2(N) and Sgr B2(M), and no adequate fit can be obtained in neither N nor M using the standard model. Therefore, a different model was applied in N and M, in which the emission originates from an extended cloud component (referred to as the "halo"), with rotation temperature T_1 and optical depth τ_1, surrounding a compact component (referred to as the "core"), with rotation temperature T_2, optical depth τ_2, and beam-filling η_{bf}. The antenna main-beam brightness temperature resulting from such a core-halo model can be expressed as

$$\begin{aligned} T_{mb} = {} & (1-\eta_{bf})[J_\nu(T_1) - J_\nu(T_{bg})](1-e^{-\tau_1}) \\ & + \eta_{bf}\{J_\nu(T_1)(1-e^{-\tau_1/2})[1+e^{-(\tau_1/2+\tau_2)}] \\ & + J_\nu(T_2)(1-e^{-\tau_2})e^{-\tau_1/2} \\ & + J_\nu(T_{bg})e^{-(\tau_1+\tau_2)} - J_\nu(T_{bg})\}\,, \end{aligned} \tag{13}$$

where τ_1 and τ_2 are calculated according to equation (4) for column densities N_1 and N_2, respectively. On account of its large number of free parameters as compared to the standard model, this model can only be used when the data clearly show two temperature components. It is also more difficult to find a unique solution, since several combinations of parameters can give approximately equally good χ^2_ν.

Using this two-component model, we found reasonable agreement with CH_3OH data in N using a temperature of 45 K and a column density of 1.0×10^{16} cm^{-2} for the halo, together with 238 K and 5.0×10^{18} cm^{-2} for the core component. The beam-filling factor was 0.008 for the core. In M we found 40 K and 1.0×10^{16} cm^{-2} for the halo, together with 150 K and 7.9×10^{18} cm^{-2} for a beam-filling factor of 0.002 for the core. The halo is optically thin, while optical depths around 8 are reached in the core. We note the possibility for the rotational-torsional transitions to be excited by radiation around 50 μm and, hence, to be in nonequilibrium with the ground state lines (see Lovas et al. 1982). In NW an adequate fit was obtained with the standard, single-component model, since only two or three high-energy (>100 K) lines were (tentatively) detected. The rotation temperature deduced, 16 K, is among the lowest in the survey, and the beam-averaged column density is 7.6×10^{15} cm^{-2}, which is similar to the halo component in N and M. One unassigned line in NW, U241719, is most likely due to either the $5_0 \rightarrow 4_0$ or the $5_{-1} \rightarrow 4_{-1}$ E transition of CH_3OH at an odd velocity (35 km s^{-1} or 127 km s^{-1}, respectively).

The $^{13}CH_3OH$ isotopomer was detected through quite a large number of lines toward N, including a few lines from the torsionally excited state. Using the same rotation temperatures and beam-filling as found for the main isotopomer, 45 and 238 K, we arrive at column densities of 7.9×10^{14} cm^{-2} and 1.0×10^{18} cm^{-2} for the halo and core component in N, respectively. The $CH_3OH/^{13}CH_3OH$ column density ratios become 13 in the halo and 5 in the core. The low ratio in the core is uncertain, since many of the lines in the 300–500 K range of the main isotopomer are considerably stronger than predicted by the model, and the fit is therefore somewhat poor, in particular in N. Also in M lines from $^{13}CH_3OH$ were detected, and a fit using a rotation temperature of 40 K gives a column density of 5.1×10^{14} cm^{-2}, which yields a $CH_3OH/^{13}CH_3OH$ column density ratio of 20 in the halo component.

We have also tentatively identified a few lines from $CH_3^{18}OH$ and CH_3OD, but we refrained from estimating column densities because of the large uncertainty in these line assignments.

4.31. CH_3CN

The $J = 12 \rightarrow 11$, $J = 13 \rightarrow 12$, and $J = 14 \rightarrow 13$ rotational bands of the symmetric-top methyl cyanide, CH_3CN, were covered by our survey. In the ground state, lines with projected quantum number K up to 12 were detected. Toward N and M, a large number of lines in the lowest excited vibrational state of CH_3CN, the doubly degenerate v_8 CCN bending mode at 520 K above the ground state, were also detected.

An analysis including both the ground and excited states yields a rotation temperature of 352 K and a beam-averaged column density of $4.2 \times 10^{15-2}$ in N, and 254 K and 7.9×10^{14} cm^{-2} in M. In NW ground state lines with K up to 3 were detected, resulting in a rotation temperature of 46 K and column density of 2.6×10^{13} cm^{-2}. Using both the ground state and v_8 data we were unable to obtain a statistically significant value for the beam-filling factor. However, by excluding the lines from the v_8 vibrational state, which can easily be excited by far-infrared radiation (e.g., Goldsmith et al. 1983), the best fit to the data is obtained for a small beam-filling factor in N and M. For η_{bf} values of 0.014 and 0.005, the rotation temperatures and column densities for N and M become 400 K and 304 K, and 6.3×10^{17} cm^{-2} and 3.1×10^{17} cm^{-2}, respectively. The maximum optical depth resulting from these models are about 1–2, which may still be somewhat low. The higher rotation temperatures obtained for the ground state lines only as compared to the ground and vibrational states together suggest that the v_8 emission is more beam-diluted. Hence, we consider the homogeneous source model used here to be oversimplistic for analyzing the CH_3CN emission from the complex Sgr B2 core region.

The two ^{13}C isotopomers were detected in N and M. Because of the small difference between the rotational constants of $CH_3^{13}CN$ and the main isotopomer most of the K-components of these species are overlapping. Hence, the line parameters of $CH_3^{13}CN$ are somewhat less well determined than those of $^{13}CH_3CN$. The column density of $^{13}CH_3CN$, assuming a rotation temperature and beam-filling factor equal to that of the main isotopomer, is 7.2×10^{16} cm^{-2} in N, and 2.5×10^{16} cm^{-2} in M. For $CH_3^{13}CN$, the column density becomes 1.1×10^{17} cm^{-2} in N. No useful estimate could be obtained from the three lines detected toward M. The corresponding $^{12}C/^{13}C$ column density ratios are 9 and 6 in N, and 12 in M, probably indicating that optical depth effects have not been fully accounted for. Three lines of $CH_3C^{15}N$ were tentatively identified toward N. However, the $13_0 \rightarrow 12_0$ line at 231.94 GHz is coincident and probably blended with a CH_3OCHO b-type line, and the $14_0 \rightarrow 13_0$ line at 249.78 GHz is located in a band with a somewhat questionable baseline. Using the remaining $13_2 \rightarrow 12_2$ integrated intensity and adopting the rotation temperature of the main isotopomer (398 K) yields a beam-averaged $CH_3C^{15}N$ column density of 9.7×10^{14} cm^{-2}. Scaling this to $\eta_{bf} = 0.014$ yields a column density of 7.5×10^{16} cm^{-2}, and a

$CH_3CN/CH_3C^{15}N$ ratio of only 9. Hence, the identification of $CH_3C^{15}N$ seems questionable.

4.32. NH_2CHO

Formamide, NH_2CHO, was detected toward N and M. This molecule has components of its dipole moment along both its *a*- and *b*-axes ($\mu_a = 3.62$ D, $\mu_b = 0.85$ D) and is one of the molecules observed for which the intrinsically weaker *b*-type transitions are anomalously strong compared to the *a*-type transitions. Therefore, *a*-type and *b*-type lines were analyzed separately in N, where 23 out of 53 detected NH_2CHO lines are *b*-type.

A good fit to the *a*-type lines in N is achieved with a rotation temperature of 175 K and a beam-averaged column density of 5.6×10^{14} cm^{-2}. Three of the lines do not fit the model at all, but are approximately 100 times stronger than predicted. These are intrinsically weak *Q*-branch lines, contrary to all other *a*-type lines which are all *R*-branch. Two of them are low-energy $\Delta K_a = 2$ transitions. The *b*-type transitions, which are *P*-, *Q*-, and *R*-branch, are less well fitted to a model because of their larger scatter, but yield a rotation temperature of 302 K and a column density as large as 9.3×10^{15} cm^{-2}. In M a rotation temperature of 145 K and a beam-averaged column density of 2.4×10^{14} cm^{-2} gives a reasonable fit to the data, with the exception of the two *b*-type transitions detected, both of which are factors of 20 and 80 too strong compared to model. In NH_2CHO the first excited state of the inversion of the NH_2 group lies at 416 K above the ground vibrational state and could therefore be significantly populated in N and M, but to our knowledge no spectroscopic data for the rotational lines in the excited state are available.

4.33. CH_3SH

Methyl mercaptan, CH_3SH, was detected in N and M. This molecule is, similarly to methanol, a near-prolate symmetric top and therefore only the prolate (K_a) pseudo–quantum number is used to label the transitions. It has *A* and *E* torsional substates, both of which have been detected. Because of a computing error the *A*-coefficients for CH_3SH listed in Table 35 of Paper I are too small. The correct *A*-coefficients can be obtained by multiplying the listed values by 5.263 for the $J = 9 \rightarrow 8$ transitions, and by 4.762 for the $J = 10 \rightarrow 9$ transitions. The rotation temperatures deduced for N and M are very similar, 35 and 41 K, and the beam-averaged column densities become 1.1×10^{15} cm^{-2} and 7.8×10^{14} cm^{-2}, respectively.

4.34. CH_3NH_2

The rotational levels of methylamine, CH_3NH_2, are split into *A* and *E* species by the internal rotation of the CH_3 group. The inversion of the NH_2 group further splits each level of both species into symmetric and asymmetric levels, with the statistical weights of the asymmetric levels being 3 times those of the symmetric levels. In N around 30 transitions (disregarding significantly blended ones) from all four substates were detected, but we note that the transitions with highest predicted line-strengths fall outside the observed frequency band.

The best fit to the data is obtained with a beam-filling factor of 2.2×10^{-3}, which results in a rotation temperature of 230 K and a column density of 1.5×10^{19} cm^{-2}. The small value of the beam-filling factor is statistically rather well determined. Because of the relatively small range of upper-state energies in the lines detected and the scattered appearance of the rotation diagram, the rotation temperature is rather poorly constrained. For comparison, in the case of $\eta_{bf} = 1.0$, i.e., beam-averaged quantities, the best-fitting rotation temperature is 148 K and the column density 7.9×10^{15} cm^{-2}.

The surprisingly large column density inferred is due to the combined effect of rather low *A*-coefficients in the detected transitions, the very large partition function of this molecule, and the high rotation temperature found. Turner (1991) infers a column density toward Sgr B2(OH) which is more than 100 times lower than our beam-averaged estimate. Furthermore, Turner points out that he failed to detect previously claimed CH_3NH_2 lines (Kaifu et al. 1974). However, as noted by Turner, all five hyperfine lines of the $2_{0,2} \rightarrow 1_{1,0}$ line have been detected. The column density inferred from this low-energy line is larger than 10^{16} cm^{-2} for $T_{rot} \gg 18$ K.

4.35. CH_3C_2H

Methyl acetylene or propyne, CH_3C_2H, is a symmetric-top molecule similar to CH_3CN, but with a much lower dipole moment. The $J = 13 \rightarrow 12$, $J = 14 \rightarrow 13$, and $J = 15 \rightarrow 14$ transitions are detected through *K* up to 6. In N and M the data are consistent with a single temperature. The resulting rotation temperatures are 214 and 87 K, and the corresponding beam-averaged column densities are 1.3×10^{16} cm^{-2} and 7.8×10^{15} cm^{-2} in N and M, respectively. Toward NW the best-fit rotation temperature is 120 K and the column density is 1.4×10^{15} cm^{-2}. The surprisingly high, and very uncertain, rotation temperature deduced in NW is probably a result from blending of high-velocity emission in the $K = 0$ and $K = 1$ with the $K = 2$ and $K = 3$ components, hence causing the intensity in the higher *K* levels to be overestimated. We also note the lack of available lines below $E_u = 75$ K. One transition from $^{13}CH_3C_2H$ was tentatively detected in N.

4.36. CH_3CHO

Acetaldehyde, CH_3CHO, has dipole moments both along its *a*- and *b*-axes ($\mu_a = 2.42$ D, $\mu_b = 1.27$ D) and, hence, exhibits *a*- and *b*-type transitions, both of which were detected toward N. We have also tentatively detected an odd *c*-type transition, which is forbidden in the strict sense. This type of transition arises as a result of the internal rotation of the CH_3 group relative to the framework of the molecule (see also discussion on CH_3OCHO below). Moreover, 18 lines in the first and second excited torsional states in the 276–565 K range were detected in N, and a single torsionally excited line was tentatively detected in M.

The *a*- and *b*-type transitions were analyzed separately in N, since they occupy two separate regions in the rotation diagram. The rotation temperature using the *a*-type lines becomes 434 K, and the beam-averaged column density is 1.6×10^{15} cm^{-2}. However, if the lines in the torsionally excited states, i.e., all *a*-type lines above 200 K, are excluded the rotation temperature and column density become 59 K and 4.4×10^{14} cm^{-2}. Since the ground and torsionally excited states are connected by torsion-rotation transitions in the far-infrared, the torsionally excited levels may be radiatively populated, which could explain the higher rotation temperature of the high-energy lines. For the *b*/*c* lines the best-fit temperature is very high, 520 K, but uncertain,

and the column density is 3.2×10^{16} cm^{-2}. This is an order of magnitude higher than derived for the *a*-type transitions, and we will discuss this issue further in § 5.2.

In M the transitions, which are all *a*-type, are well described by a low rotation temperature, 47 K, and a column density of 2.7×10^{14} cm^{-2}, which is very similar to what was found for the ground-state *a*-type transitions in N. The single torsionally excited line is several orders of magnitude too strong compared to this model, which may indicate either a misidentification or "anomalous" excitation similar to that in seen N.

4.37. *c*-C_2H_4O

Ethylene oxide, *c*-C_2H_4O, is a structural isomer to CH_3CHO having a C—O—Cring configuration, and was first identified in Sgr B2(N) by Dickens et al. (1997) using data from this survey, Haystack Observatory, and Nobeyama Radio Observatory. They obtained a rotation temperature of 18 K and a column density averaged over a 20″ beam of 3.3×10^{14} cm^{-2}. Ethylene oxide has subsequently been confirmed in a number of additional hot-core sources (Nummelin et al. 1998b).

4.38. C_2H_3CN

Vinyl cyanide (acrylonitrile), C_2H_3CN, was detected through its *a*- and *b*-type transitions toward N, and mainly through its *a*-type transitions toward M. In N also a large number of rotational transitions in the two lowest-lying excited CCN bending modes were identified. A detailed analysis of the C_2H_3CN data in the N position in terms of a core-halo structure was carried out and was published separately (Nummelin & Bergman 1999). They obtained a beam-averaged column density of 1.0×10^{15} cm^{-2} in the "halo," where the kinetic temperature varies between 18–180 K. The warm core was best modeled by a rotation temperature of 440 K and a column density of 5.1×10^{18} cm^{-2} for a beam-filling factor of 10^{-3}. In M a fit to the *a*-type lines yields a rotation temperature of 350 K and a beam-averaged column density of 4.2×10^{14} cm^{-2}.

4.39. CH_3OCHO

Methyl formate, CH_3OCHO, is the molecule with the largest number of lines ($\sim$250) detected in this survey. Besides the normal *a*- and *b*-type transitions this molecule also has forbidden transitions that obey either the *c*-type selection rules, or none of these rules (*x*-type). This is due to mixing of states through the internal rotation of the CH_3 group with respect to the framework of the molecule (Plummer, Herbst, & De Lucia 1987), and, similar to the *b*-type lines, these transitions are intrinsically weaker than the *a*-type lines. In N all of these types of transitions were detected, and in the analysis they were divided into two groups.

No rotation temperature could be determined for the *a*-type transitions in N, and a value of 200 K was therefore used. The resulting column density is 5.6×10^{15} cm^{-2}. In M the rotation temperature and column density are 240 K and 1.6×10^{15} cm^{-2}, respectively. For the *b*/*c*/*x*-type lines in N, a rotation temperature of 500 K was assumed since no useful value could be obtained from fitting. This yields a column density of 4.0×10^{16} cm^{-2}. The fits for CH_3OCHO are rather poor, partly owing to the large number of weak lines. The somewhat low-lying fits shown in the rotation diagrams is a consequence of the fitting method used (see discussion in § 3).

It should be noted that CH_3OCHO has an excited torsional state at about 190 K above the ground state, which is likely to be significantly populated in the cores of Sgr B2. This would also affect the molecular partition function and, hence, the total column density. However, no spectroscopic data for the rotational lines in the torsionally excited states of CH_3OCHO are available to the best of our knowledge.

4.40. C_2H_5OH

Owing to the motion of the H atoms relative to the OH group ethanol, C_2H_5OH, has three different torsional substates in its ground vibrational state. The lowest-energy conformation is the trans form, with the gauche+ form offset by 57 K above the trans form, and the gauche− form offset by 62 K. Transitions within the trans form occur as *b*-type and very weak *a*-type, while transitions within either of the gauche forms are *a*-type and weak *b*-type, and transitions between the two gauche forms are strictly *c*-type. All of these types of transitions except *a*-type trans lines were detected toward the N and M positions. The rotation temperatures deduced are 73 and 60 K, and the beam-averaged column densities are 4.2×10^{15} cm^{-2} and 1.1×10^{15} cm^{-2} in N and M, respectively. Toward NW a few trans lines were detected, yielding a rotation temperature of 40 K and a column density of 1.0×10^{15} cm^{-2}. The large number of detected lines from ethanol in its gauche conformations shows the importance of accounting for these states in the partition function (Pearson et al. 1997), which could otherwise be significantly underestimated.

4.41. CH_3OCH_3

Dimethyl ether, CH_3OCH_3, has two internal rotors which cause splitting into four torsional substates, denoted *EE*, *AA*, *EA*, and *AE*. This splitting is unresolved in most of the lines observed in the survey and is only partly resolved in a few of the lines. In N the best-fitting rotation temperature is 197 K, and the beam-averaged column density is 7.9×10^{15} cm^{-2}. In M, the range of energies of the detected lines is rather narrow (48–159 K) and the scatter of the data points in the rotation diagram is large. Therefore, both the estimated rotation temperature of 150 K and the column density of 3.4×10^{15} cm^{-2} are uncertain.

4.42. C_2H_5CN

Ethyl cyanide (propionitrile), C_2H_5CN, was detected in N through a large number of *a*- and *b*-type lines, and in M through *a*-type lines and a single *b*-type line (at 37 K). In addition to the ground state lines previously assigned in Paper I, very recent laboratory spectroscopy (Pearson 1999, private communication) has allowed some 90 rotational lines in the first torsionally excited state and the excited CCN in-plane bending mode of C_2H_5CN to be assigned in N. The identification and analysis of these data will be described in a forthcoming paper. An analysis based on the ground state lines only gives a rotation temperature and beam-averaged column density of 175 K and 1.6×10^{15} cm^{-2}, respectively, for the *a*-type transitions. For the *b*-type lines we find 210 K and 1.5×10^{16} cm^{-2}. In M, we estimate a rotation temperature of 146 K and a beam-averaged column density of 2.2×10^{14} cm^{-2}.

4.43. *Recombination Lines*

Three recombination lines of hydrogen were clearly detected toward M, and one toward N. The strongest of these is the H30α transition. This line is rather broad in M, 30 km s^{-1} (FWHM), and also seems to have line wings extending to 100 and 25 km s^{-1} on the high and low velocity side, respectively. In N the H30α line has two approximately equally strong velocity components, at 60 and 72 km s^{-1}. The H38β and H37β lines are both comparatively broad but weak features. The H29α line at 256,302 MHz is lost under lines from CH_3C_2H. The weaker He29α and He30α lines at 256,406 and 231,995 MHz, respectively, were not detected.

4.44. *Kinematics*

Toward Sgr B2(N) the emission velocities with respect to the local standard of rest (V_{LSR}) are remarkably constant among the different molecules, with the average velocity at 63.7 km s^{-1}. Only H_2CO has a somewhat lower average emission velocity, 60.8 km s^{-1}, which may in part be due to self-absorption. The average line width in N is 13 km s^{-1} (FWHM).

In Sgr B2(M) the emission velocity varies somewhat more than in N around the average of 61.6 km s^{-1}. A general trend in the data is that the larger molecules, such as C_2H_3CN, C_2H_5CN, CH_3CHO, CH_3OCH_3, CH_3OH, and NH_2CHO, have higher emission velocities, 64–65 km s^{-1}, than the other species. Furthermore, a few smaller molecules, including HNC, SO, SO_2, NS, NO, H_2CO, and C_3H_2, have somewhat lower velocities, 55–60 km s^{-1}, than average. The line width in M is on the average 17 km s^{-1} (FWHM).

Toward the Sgr B2(NW) position, most molecules have two or more visible velocity components, and in many lines the components are equally strong. This can be clearly seen in, for example, the $4_2 \rightarrow 3_1$ (at 218.44 GHz) and the $5_0 \rightarrow 4_0$ (at 241.79 GHz) E transitions of CH_3OH, and the $10_{0,10} \rightarrow 9_{0,9}$ transition of HNCO, all of which have two components at 57–59 km s^{-1} and 72–74 km s^{-1}. In the majority of the species the peak of the emission occurs at about 70 km s^{-1}.

4.45. *Isotopomeric Column Density Ratios*

In order to estimate column density ratios from observations of isotopomers, more detailed analyses allowing for gradients in excitation and physical conditions would be required in most cases. Most of the isotopomeric column density ratios listed in Table 2, being lower or much lower than the expected values in the Galactic center region (Wilson & Rood 1994), seem to reflect underestimated optical depths in the main isotopomers and in some cases also in the rarer ones. One exception is the $HC^{18}O^+/HC^{17}O^+$ ratio in Sgr B2(M), which is 6.6 ± 2.8 and accordingly is almost a factor 2 higher than expected from the $^{18}O/^{17}O$ ratio of 3.6 estimated by Penzias (1981). Our observed $C^{18}O/C^{17}O$ column density ratios are 3–4, but an optical depth greater than 1 in the $C^{18}O$ $J = 2 \rightarrow 1$ line cannot be ruled out. The most reliable isotopic ratio inferred from the survey analysis should be the $^{32}S/^{34}S$ ratio of approximately 20, determined through the $^{32}SO_2/^{34}SO_2$ and $^{32}SO/^{34}SO$ ratios. Also the $^{34}S/^{33}S$ ratio inferred from the $C^{34}S/C^{33}S$, $^{34}SO/^{33}SO$, and $^{34}SO_2/^{33}SO_2$ isotopomeric ratios, 3.3–5.7, seems to be in fair agreement with the ratio of 6.3 found by Chin et al. (1996) for Galactic disk molecular clouds.

The $^{16}O/^{18}O$ abundance ratio as estimated from the $SO/S^{18}O$ and $SO_2/SO^{18}O$ column density ratios is consistent: 120^{+58}_{-54} and $2 \times 56^{+13}_{-11} = 112^{+26}_{-22}$, respectively. Taken together, this suggests a $^{16}O/^{18}O$ abundance ratio which is a factor of 2 lower the canonical value of 250 for the Galactic center region (Wilson & Rood 1994). The canonical value is based on absorption measurements of OH and H_2CO (e.g., Whiteoak & Gardner 1981; Henkel et al. 1983). Absorption observations by Gardner et al. (1989) using the $2_0 \rightarrow 3_{-1}$ line of $CH_3^{18}OH$ at 11.6 GHz also supports a $^{16}O/^{18}O$ abundance ratio close to the canonical value. However, all these estimates are based on absorption measurements and reflect the condition in the foreground gas. Our estimate is related to a small source ($\sim$0.12 pc) in the M core, and could therefore be directly connected to recent star-forming activities. The current view is that ^{18}O only is enhanced relative to ^{16}O in massive stars ($>10\ M_\odot$) and brought into the interstellar medium by Wolf-Rayet winds and/or supernova explosions (Prantzos, Aubert, & Audouze 1996). Thus, our low value of the $^{16}O/^{18}O$ abundance ratio may indicate that the births (and deaths) of massive stars have affected the $^{16}O/^{18}O$ abundance ratio in the very core of Sgr B2(M). Indeed, the high-resolution studies of the ionized gas by De Pree, Goss, & Gaume (1998) indicate the presence of some 20 B0–O6 stars.

5. DISCUSSION

5.1. *Determination of Fractional Abundances*

5.1.1. H_2 *Column Densities*

To determine the true fractional abundance of a certain molecular species relative to H_2, which can be compared to abundances calculated in time-dependent chemical models, the number density of the species observed as well as that of H_2 must be known in the probed interstellar gas. The determination of number densities requires, in most cases, the solution of the coupled radiative transfer and statistical equilibrium equations, which in turn requires knowledge of the source structure and of the collisional rate coefficients. In practice the determination of molecular fractional abundances therefore usually relies on column densities rather than number densities, since the former are more directly related to the observed integrated line intensities. However, differences in excitation and variations in the fractional abundances and small-scale distribution of the molecular gas, e.g., due to photodissociation, could all be significant sources of errors in the ratios of column densities of different species. Hence, even if the beam-averaged molecular column density is compared with an H_2 column density determined for a similar angular resolution, the excitation and abundance variations in the plane of the sky as well as along the line of sight make fractional abundances determined from beam-averaged column densities rather uncertain. For the molecular column densities determined from a single transition the unknown rotational temperature is of course a large source of error (see the discussion of abundance determination in Irvine et al. 1985).

Hence, it is clear that a proper choice of H_2 column density is critical in order to obtain accurate relative abundances. Numerous estimates of the H_2 column density in the cores of Sgr B2 have been made, and some recent results are summarized in Table 5. Most of them are based on

TABLE 5

ESTIMATES OF THE H_2 COLUMN DENSITIES IN SGR B2

TRACER	RESOLUTION	N (10^{24} cm^{-2}) Sgr B2(N)	Sgr B2(M)	Sgr B2(NW)	REFERENCE
Continuum.....	23″	3.5	2.2	...	GSL87
NH_3	5″ × 3″	10	0.1	...	VGP87
Continuum.....	4.″5 × 2″	4	...	...	CV89
Continuum.....	84″	...	1.4–64	...	LG89
Continuum.....	23″	...	2.6	...	LG90
Continuum.....	12″	5	1	...	MVWJ90
$C^{17}O$	20″	...	2.2	...	SJDB91[a]
Continuum.....	9–13″	15	4.3	...	G93
NH_3	4″	10	10	...	HWHM93
Continuum.....	4.″5 × 3.″7	11	5	...	LGCS93
Continuum.....	15″ × 5″–10″ × 4″	80	2	...	KMS96
CH_3CN	16–20″	5	4	...	dVMW97
$C^{17}O$	23″	2.8	3.5	0.6	This work[a]

[a] Using $X(C^{18}O) = 6.0 \times 10^{-8}$ (Lis & Goldsmith 1989) and $X(C^{18}O)/X(C^{17}O) = 3.6$ (Penzias 1981).

REFERENCES.—GSL87: Goldsmith, Snell, & Lis 1987b; VGP87: Vogel, Genzel, & Palmer 1987; CV89: Carlstrom & Vogel 1989; LG89: Lis & Goldsmith 1989; LG90: Lis & Goldsmith 1990; MVWJ90: Martín-Pintado et al. 1990; SJDB91: Sutton et al. 1991; G93: Gordon et al. 1993; HWHM93: Hüttemeister et al. 1993; LGCS93: Lis et al. 1993; KMS96: Kuan, Mehringer, & Snyder 1996; dVMW97: de Vicente, Martín-Pintado, & Wilson 1997.

continuum flux measurements that yield the dust optical depth, dust column density, and ultimately, assuming a gas-to-dust ratio, the H_2 column density. The large variations among the results can be ascribed to differences in angular resolution and in the estimated source size, as well as to differences in adopted dust emissivity and dust opacity spectral index.

A beam-averaged (23″) H_2 column density can be estimated from the $C^{17}O$ column density inferred from the integrated intensity of the $J = 2 \rightarrow 1$ line in our survey. By adopting a fractional $C^{18}O$ abundance of 6×10^{-8} in Sgr B2 (models A–D by Lis & Goldsmith [1990]) and a $C^{18}O/C^{17}O$ abundance ratio of 3.6 (Penzias 1981), we derive H_2 column densities of 3×10^{24} cm^{-2}, 4×10^{24} cm^{-2}, and 6×10^{23} cm^{-2} for Sgr B2(N), Sgr B2(M), and Sgr B2(NW), respectively. We note that the fractional abundance of $C^{18}O$ determined by Lis & Goldsmith (1990) is considerably lower than the value of 2×10^{-7} reported by Frerking, Langer, & Wilson (1982) for the ρ Oph and Taurus molecular clouds. If we use the canonical $^{16}O/^{18}O$ ratio[5] of 250, this implies a surprisingly low CO abundance in Sgr B2 (2×10^{-5}). Adopting a more "normal," i.e., higher, CO abundance would decrease the H_2 column densities by a factor of 3–5.

Zmuidzinas et al. (1995) formulate the following expression for the gas density in Sgr B2 as a function of radius based on model C by Lis & Goldsmith (1990):

$$n_{H_2}(r) = n_1 + n_2\left(\frac{r}{22.5 \text{ pc}}\right)^{-2}, \quad (14)$$

where $n_1 = 2.2 \times 10^3$ cm^{-3}, $n_2 = 170$ cm^{-3}, and $r \leq 22.5$ pc. This density model yields a column density of 3×10^{24} cm^{-2} in a 23″ beam, in agreement with our $C^{17}O$ results toward Sgr B2(N). At a position 46″ away from the cloud center, which is the angular distance between Sgr B2(NW) and Sgr B2(N), the beam-averaged column density becomes 7×10^{23} cm^{-2}, also in agreement with our $C^{17}O$ data. For Sgr B2(M) we used the same density law as above, but with $n_2 = 93$ cm^{-3}, which gives better agreement with observed column densities toward this position (Table 5 and Fig. 3).

Based of the agreement between the H_2 column density resulting from the above density models and the estimates listed in Table 5, including our $C^{17}O$ data, we adopt the H_2 column densities for Sgr B2(N) and Sgr B2(M) given by the convolution of a source which has a radial density distribution described by equation (14) with a Gaussian corresponding to the angular resolution. For an angular resolution of 23″, the H_2 column densities thus become 3×10^{24} cm^{-2} toward Sgr B2(N) and 2×10^{24} cm^{-2} toward Sgr B2(M). The H_2 column density as a function of the angular resolution is displayed in Figure 3 for Sgr B2(N) and Sgr B2(M). It should be stressed, however, that for angular resolutions less than a few arcseconds the $N(H_2)$ relations are extrapolations from observations at coarser angular resolutions. For Sgr B2(NW) we use the H_2 column density deduced from our $C^{17}O$ data, 6×10^{23} cm^{-2}. These H_2 column densities, determined for the appropriate angular resolution, together with the column densities listed in Table 1 have been used to calculate molecular fractional abundances relative to H_2. The abundances are summarized in Table 3.

5.1.2. "*Beam-averaged*" *vs.* "*True*" *Abundances*

It is not straightforward to compare the fractional abundances obtained from beam-averaged column densities with those obtained from column densities valid for small ($\ll$23″) source-sizes, even when the H_2 column densities used to calculate the abundances have been calculated according to the relation displayed in Figure 3. The reason is that they scale differently, since the H_2 cloud is spatially resolved while the molecular emission region in question is unresolved. As long as the molecular line emission stays opti-

[5] Using our value of 120 from SO and SO_2 from § 4.45 to derive CO abundances is not appropriate since it refers to a small source (2.″9).

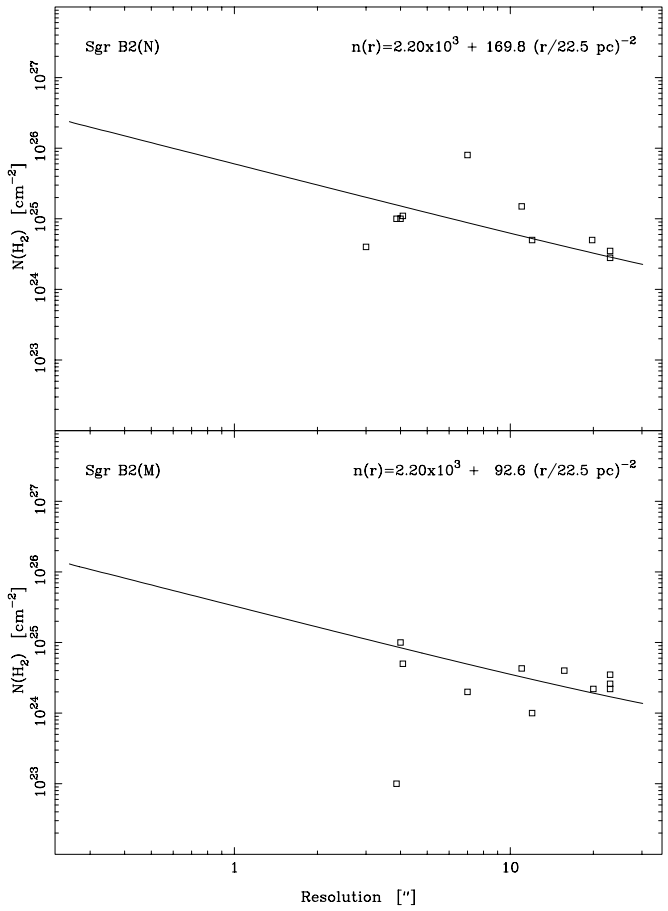

FIG. 3.—H_2 column density as a function of angular resolution for Sgr B2(N) and Sgr B2(M), respectively. Observed values (Table 4) have been indicated with squares. The curves were calculated by convolving the density distribution (eq. [14]) with a Gaussian corresponding to the angular resolution

cally thin, the column density obtained will increase as the inverse of the beam-filling factor, i.e., approximately as the inverse of the source area. The H_2 column density, on the other hand, is calculated by convolving the H_2 number density distribution given by equation (14) with a Gaussian corresponding to the source size estimate. It therefore increases approximately as the inverse of the angular resolution and, thus, more slowly than the column density of the observed species. For example, going from $\eta_{bf} = 1$ to 10^{-2} (corresponding to a 2".3 source size) increases the estimated molecular column density by a factor 100 (still assuming optically thin emission), while the H_2 column density toward Sgr B2(N) rises by a factor of 10 from about 2.7×10^{24} cm^{-2} to 2.6×10^{25} cm^{-2}. Hence, the fractional abundance deduced from the column density referring to $\eta_{bf} = 10^{-2}$ will be approximately 10 times higher than in the beam-averaged case. Should the beam-filling factor become small enough, the correspondingly high column density will result in optically thick line emission, which leads to larger abundances than in the optically thin case.

Furthermore, the H_2 column densities shown in Figure 3 are integrated along the full line of sight through the cloud. We would expect the spatial extent of the molecular emission region to be approximately equal in all directions. Hence, species with small spatial extent in the plane of the sky should preferably be compared to H_2 column densities integrated along a small spherical core rather than along a cylindrical source extending through the entire cloud. The fractional abundances could therefore be somewhat underestimated. However, this correction would be rather small because of the r^{-2} dependence of the H_2 number density.

5.2. *The Anomalous Excitation of the Emission from Large Molecules*

From previous spectral line surveys (Turner 1991; Sutton et al. 1991) it is known that some large asymmetric molecules can exhibit "anomalous excitation." If a line having an Einstein A-coefficient significantly lower than average is detected, it will often imply a higher molecular column density than do the lines with "normal" A-coefficients. In the rotation diagram such lines will therefore lie markedly above the rest of the lines. The reason for a transition to have a lower A-coefficient can be that the transition is attributed to one of the minor molecular dipole moments (in most cases considered here μ_b or μ_c are the weaker ones), or that the transition involves a large ΔK_a and/or ΔK_c. The molecular species observed to exhibit this effect in our survey are NH_2CHO, CH_3CHO, C_2H_3CN, CH_3OCHO, and C_2H_5CN, and this effect is almost exclusively seen in Sgr B2(N). For these molecules, all observed b- and c-type transitions seem to some extent to be affected by anomalous excitation. Three possible explanations will be discussed below.

5.2.1. *Are the b-Type Transitions Misidentifications?*

Our main argument against the hypothesis that the observed lines with low A-coefficients are blends or misidentifications is the vast number of such transitions assigned both in this survey and in previous ones. In our analysis of molecules with this kind of problem we made separate χ^2-fits to the a-type and b/c-type lines. Using the rotation temperatures and column densities inferred for the b-type lines we then checked the consistency of the line identifications. The conclusion is that there are indeed a number of lines which, according to the adopted model, should have been detected but were not, despite the S/N ratio being sufficient and the spectrum being free from other emission lines. However, the number of such lines is relatively small, on the order of 10%–20%, for all of the species. The assumption of uniform excitation is anyhow a crude one, and it is therefore difficult to predict the intensities of these missing lines with high accuracy. Hence, we do not believe that the missing lines pose a serious objection to our proposed identifications of the b-type lines.

Furthermore, the general agreement between the observed frequencies and the rest frequencies of the assigned transitions is equally good for the b-type as for the a-type lines. The standard deviation (i.e., the 1 σ scatter) among the emission velocities of the observed lines is about 5–7 km s^{-1}, i.e., about half the typical line widths in Sgr B2. If the observed b-type lines were all misidentifications, we would expect them to be much more scattered in frequency/velocity than the securely identified a-type lines, which would produce a higher standard deviation. This is apparently not the case. Although some of the b-type lines may be blends with other species or even misidentifications, we believe the majority of the b-type as well as the a-type lines to be correctly identified.

Another argument against the misidentification hypothesis is that a large number of CH_3OCHO b-type transitions

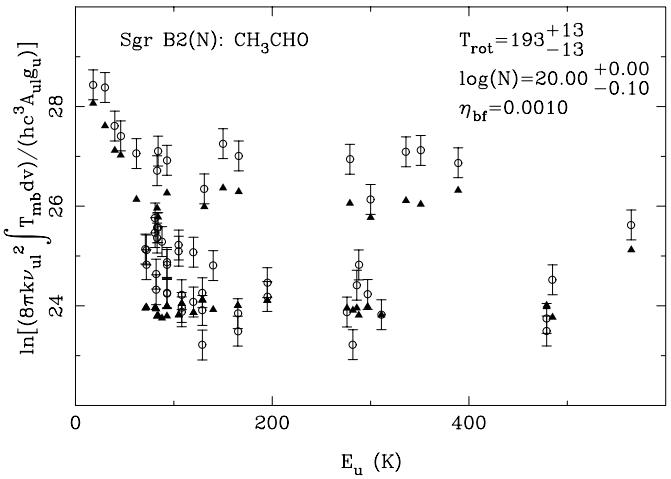

FIG. 4.—Rotation diagram with observed (*circles*) and calculated (triangles) CH_3CHO line intensities. In this model all lines are optically thick ($1.5 \leq \tau \leq 125, \eta_{bf} = 0.001, N(CH_3CHO) = 10^{20}$ cm^{-2}).

were detected in a recent SEST survey of *c*-C_2H_4O toward a number of hot-core sources (Nummelin et al. 1998b). The noise levels in these spectra are very low ($\sim$5–10 mK), and in at least two of the sources, NGC 6334F and G327.3 − 0.6, the lines are narrow (5 km s^{-1}) in comparison to Sgr B2. This significantly decreases the risk of line confusion and blends, hence allowing much more secure line identifications to be made. Nevertheless, the *b*-type lines are detected and are excessively strong in these sources as well, which suggests that this effect is common to hot molecular cloud cores and due to the molecular excitation itself.

5.2.2. *Are the Transitions Very Optically Thick?*

A second possible explanation for the intrinsically weaker (*b*-type) lines being too strong compared to the intrinsically stronger (*a*-type) ones could be that this is an effect caused by extremely high optical depths. If all lines were optically thick, their intensities would all equal the product of the rotation temperature and the beam-filling factor. In the rotation diagram, each line intensity will be scaled with the relevant *A*-coefficient, statistical weight, and frequency, and only these parameters will determine the appearance of the diagram. An example of this, in the case of CH_3CHO, is shown in Figure 4. The optical depths resulting from the model shown are between 1.5 and 125, and the source size is very small (0.″8), the beam-filling being 10^{-3} in a 23″ beam. If this were the case, most of the rare isotopomer lines would be as strong as those of the main isotopomer. The estimated CH_3CHO column density of 10^{20} cm^{-2}, together with an H_2 column density of about 10^{26} cm^{-2} estimated for a 0.″8 source (Fig. 3), implies a fractional abundance $X(CH_3CHO) = 10^{-6}$, which seems unlikely high. If we instead assume that $X(CH_3CHO) \leq 10^{-7}$, this leads to $N(H_2) \geq 10^{27}$ cm^{-2}. Because of the extreme combination of source size and column density required to reproduce the appearance of the CH_3CHO rotation diagram, we do not believe such a model to be physically plausible. Hence, we find it hard to believe that optical depths alone could explain the excessively strong *b*-type lines.

5.2.3. *Are the b-Type Transitions Radiatively Pumped?*

Turner (1991) performed detailed excitation calculations in an attempt to understand the anomalously strong *b*-type transitions observed in his survey (Turner 1989). Despite trying several different collisional coefficient schemes he was unable to model the anomalous excitation. We propose that an alternative explanation in terms of radiative pumping via rotational-vibrational far-infrared transitions definitely should be investigated. This is motivated by the fact that all molecular species which have excessively strong *b*- or *c*-type transitions also have low-lying (< 500 K) modes of vibration, connected to the ground state through transitions in the far-infrared regime (see Table 6).

For some of these molecules, rotational lines in excited vibrational states have actually been detected, e.g. C_2H_3CN (Nummelin & Bergman 1999) in the CCN bending modes, and torsionally excited CH_3CHO (see § 4), thus confirming that such states are in fact considerably populated in Sgr B2(N). It is also worth noting that the emission from rotational lines in vibrationally or torsionally excited states as well as the anomalous excitation is much more prominent in Sgr B2(N) than Sgr B2(M) (although also seen in Sgr B2(OH); see Turner 1991). The high far-infrared luminosity of Sgr B2 makes it important to consider the influence of optically thick far-infrared radiation.

5.2.4. *Which Transitions Give Reliable Column Densities?*

For the molecular species studied in this paper the column densities resulting from using only *b*-type transitions are between 4 and 70 times larger than those derived using only *a*-type transitions (see Table 6). The rotational temperatures derived from *b*-type transitions are also always higher. Based on the previous discussion we argue that the rotation temperatures and column densities resulting from fits to the *a*-type transitions alone are likely to give more correct results. The only case where this may not be true is if the *a*-type lines were optically thick, in

TABLE 6

LOWEST FUNDAMENTAL VIBRATIONS OF COMPLEX MOLECULES HAVING ANOMALOUSLY STRONG *b*-TYPE TRANSITIONS

Species	E_u (K)	λ (μm)	Vibrational Mode	N_b/N_a
NH_2CHO.....	416	35	NH_2 inversion	16
CH_3CHO	207	46	CH_3 torsion	72
C_2H_3CN	344	42	CCN in-plane bend	4.0
CH_3OCHO.....	190	77	CH_3 torsion	7.2
C_2H_5CN	297	48	CCN in-plane bend/CH_3 torsion	9.4

NOTE.—E_u is the energy difference between the $0_{0,0}$ level in the ground and vibrationally excited states; N_b/N_a is the ratio in Sgr B2(N) between column densities inferred from *b*-type and *a*-type transitions, respectively.

which case the more optically thin *b*-type lines could give a better estimate of the (high) column density. Although we do not exclude the possibility that the emission from these molecules can be moderately optically thick, we argue that this does not provide the full explanation to the anomalously strong *b*-type transitions. Caution is needed in particular when interpreting data for which the *a*-type and *b*-type lines sample entirely different energy regimes, since in this case (e.g. C_2H_3CN) it is not obvious whether the *b*-type transitions have anomalously large intensities or simply sample different regions in the source (Nummelin & Bergman 1999).

5.3. *Physical Structure and Molecular Excitation*

In this paper the molecular excitation problem has been decoupled from the radiative transfer problem by assuming that the population of the energy levels of each individual molecular species can be described by a single Boltzmann distribution.[6] The radiative transfer problem was subsequently solved by assuming a homogeneous, uniformly excited source. The free parameters have thus been the rotational excitation temperature, the molecular column density, and the effective beam-filling factor of the molecular line emission. Despite the fact that more than one physical source component is present in the 23″ SEST beam, the analysis shows that for many species this approach seems to give reasonably consistent results. Toward the Sgr B2(NW) position almost all of the species detected can be successfully analyzed with this model. In Sgr B2(N) and Sgr B2(M) two good examples are SO and SO_2, for which good fits to the data from several isotopomers were obtained. For a number of species, again most notably SO and SO_2 but also NO, NS, H_2CS, CH_2NH, HC_3N, CH_3CN, and CH_3OH, the optical depths are larger or considerably larger than unity, and analyses assuming optically thin emission will give poor results. Also, the isotopomeric ratios indicate optically thick emission in a number of additional species, mostly the diatomic and linear triatomic molecules.

For most species the highest rotation temperatures are found in Sgr B2(N). In Sgr 2(M) only SO_2 exhibits a significantly higher rotation temperature as compared to Sgr B2(N). Here it should be noted that underestimated optical depths can lead to overestimated rotation temperatures. However, we find that the estimates of the molecular column densities in many cases do not critically depend on the rotation temperature, which is sometimes poorly constrained by the data. In Sgr B2(NW) the temperatures for most molecules fall in the range 15–50 K. Such emission from gas of low excitation is also present toward the Sgr B2(N) and Sgr B2(M) positions. Molecules indicating such low rotation temperatures (15–70 K) are C_3H_2, CH_3OH, CH_3SH, HNCO, CH_3CHO, and C_2H_5OH. For CH_3OH, HNCO, and CH_3CHO high-energy transitions indicate 150–300 K. In one case, CH_3OH, we tried a first step toward a model with physical gradients by adopting a core-halo model having different rotation temperatures and column densities for the two cloud components. In the case of CH_3OH, we find this two-component model to reproduce the data more accurately than the standard model.

[6] For CH_3OH in M and N we actually used two rotational temperatures, and for HC_3N in N we used different rotational and vibrational temperatures to describe the population distribution.

In fact, we could argue that all molecules seen in the NW position, which is believed to be representative for the cloud envelope surrounding the Sgr B2 core region, also should be present in the gas in which the Sgr B2(N) and Sgr B2(M) cores are embedded. Hence, the emission from these molecules cannot be described well by a single rotational temperature owing to the large differences in physical conditions in the envelope and the cores. However, the emission from the envelope may easily be hidden under the prominent emission from warm gas in the cores, so that we fail to recognize this cooler gas component. The opposite case, in which the emission is dominated by the envelope, may also exist (*c*-C_3H_2 could represent such a case).

The molecular species seen in vibrationally or torsionally excited states are: SO_2, CH_3CN, C_2H_3CN (skeletal bending modes), CH_3OH, CH_3CHO (CH_3 internal rotation), HC_3N (skeletal bending modes and C—C stretch), and NH_2CN (NH_2 inversion). The vibrationally excited lines, offset 70–1240 K above the ground vibrational states, obviously trace highly excited gas, and in some of the species, e.g. CH_3CN and CH_3CHO, it is difficult to obtain a good fit to the intensities of the ground-state lines simultaneously with the vibrationally excited lines. This can be understood in terms of different beam-filling factors and excitation temperatures. Since the cores of Sgr B2 are extremely luminous at far-infrared wavelengths (e.g., Goldsmith et al. 1992; Xie et al. 1993), radiative excitation by optically thick far-infrared radiation may be the most plausible mechanism for populating the excited vibrational states (see Goldsmith et al. 1983; Carroll & Goldsmith 1981; Nummelin & Bergman 1999).

5.4. *Chemical Characteristics*

5.4.1. *Abundances from Beam-averaged Column Densities*

As can be seen in Table 3, the fractional abundances derived from beam-averaged column densities show a rather uniform chemical composition among the three surveyed sources. In fact, some species (C_2H, HCS^+, H_2CO, HNCO, cold CH_3OH, and C_2H_5OH) even appear to be more abundant by up to a factor of about 3 in the Sgr B2(NW) position as compared to the two core positions Sgr B2(N) and Sgr B2(M). This could, of course, be a result of the adopted beam-averaged H_2 column densities (see § 5.1), but it could also be explained by higher opacity in the lines toward the core positions. In addition, as could be the case for cold CH_3OH and C_2H_5OH, the emission from a high column density source with low T_{rot} in NW could also be present in N and M but may be partly lost under the warmer, and more intense, emission in the directions of the cores. Hence, for most of the molecular abundances based on beam-averaged column densities, we cannot state that small differences between the three positions are actually due to different chemical compositions.

However, there are a few exceptions. The ion SO^+ was only detected in M, while $HCNH^+$ is only seen in the quiescent NW position. Also, the $HOCO^+$ ion seems to be factor of 3–4 more abundant in NW as compared to N and M. Two other exceptions are the abundances of H_2CS and CH_2NH. If we convert the abundances in N to beam-averaged values we still find that they both are about a factor of 5 more abundant in N than in M and NW. Moreover, the molecules CH_2CN, HCOOH, CH_3NH_2, and *c*-C_2H_4O are only seen in N, although in these cases our

failure to detect these molecules in M and NW could simply be a result of lower beam-averaged molecular column densities in these positions.

For those species only seen in the N and M cores the situation is somewhat different. The beam-averaged abundances of the complex organic molecules NH_2CN, NH_2CHO, CH_3OCHO, C_2H_3CN, and C_2H_5CN are higher in N than in M. The abundance ratio $X(N)/X(M)$ is 2 for NH_2CHO and CH_3OCHO while for the oxygen-lacking molecules NH_2CN and C_2H_5CN the ratio is even higher, about 4 and 5, respectively. If we convert the abundance of C_2H_3CN in N, listed in Table 3, to a beam-averaged quantity we find $X(N)/X(M) = 8$.

5.4.2. *Abundances from Column Densities Corrected for Small Source Sizes*

For some molecules observed in Sgr B2(N) and (M), we were able to deduce column densities corrected for small source sizes, and thereby obtain abundances adjusted for beam-filling and high optical depth. This enables us to more accurately estimate abundance differences between N and M. For instance, it is clear that the sulphur containing molecules SO_2 and SO are more abundant in M than in N. For SO_2 the abundance ratio $X(M)/X(N)$ is 13 while for SO the ratio is 5. Also NS seems overabundant in M by a factor of 2 (if we assume the same T_{rot} for NS as found for NO in M, see § 4.6). For NO and hot CH_3OH we find $X(M)/X(N) = 1.4$ and 1.0, respectively. The abundances of HC_3N and CH_3CN are higher in N compared to M, by factors of 1.3 and 3, respectively.

For the molecules displaying high rotation temperatures we have also, for comparison, derived abundances for N and M using a fixed beam-filling factor $\eta_{bf} = 10^{-2}$ and rotation temperature $T_{rot} = 200$ K. The result from this exercise shows that, as expected, the abundances that were based on beam-averaged column densities increase by an order of magnitude owing to the smaller beam-filling factor (see § 5.1). Furthermore, the chemical similarity between N and M is emphasized, since the abundances tend to become even more equal between the two sources. An example of this is NH_2CN, the abundance of which increases from 9×10^{-11} and 2×10^{-11} in N and M, respectively, to 3×10^{-10} in both N and M. We conclude that the overabundance by more than a factor of 4 in N in this case is due to the large difference in rotation temperatures derived. In a few cases, e.g. HC_3N and CH_3CN, where the differences in abundances do not seem to be due to differences in rotation temperatures, the overabundance in N increases slightly.

5.4.3. *Comparison of Abundances*

A comparison between the abundances reported here (Table 3) and those derived by Sutton et al. (1991) from their 330-355 GHz line survey of Sgr B2(M) shows excellent agreement if we restrict the comparison to abundances that are based on beam-averaged column densities. The resolution of the data of Sutton et al. is 20″, i.e. close our beamwidth of 23″.

Ziurys et al. (1994) detected N_2O toward Sgr B2(M) and estimated an abundance of 10^{-9} in agreement with our value of 2×10^{-9}. In addition, we find the same value for the N position.

In their full synthesis observations of C_2H_5CN toward Sgr B2(N) and M, Miao & Snyder (1997) estimate a fractional abundance of 10^{-8} in the N core. They did not detect C_2H_5CN in M. Our abundances, based on beam-averaged column densities, are 5×10^{-10} and 1×10^{-10} in N and M, respectively. The C_2H_5CN source in N found by Miao & Snyder is marginally resolved by their synthesized beam of 6″.7 × 2″.7. Scaling their column density to 23″ angular resolution and using our adopted H_2 column density of 3×10^{24} cm^{-2} yields an abundance of 10^{-9}, which is in agreement with our result for N, considering the much higher rotation temperature used in our analysis. However, their 3 σ upper limit of the abundance in M is an order of magnitude lower than is inferred from our detection in this position.

It is also interesting to compare our abundances with those reported for the Orion sources by Blake et al. (1987). In a few cases the abundances found in the Sgr B2 sources are rather low as compared to Orion. C_2H is an example of this. An explanation could be that, since the C_2H emission in Sgr B2 exhibits a rather broad and asymmetric feature (Paper I), it is affected by self-absorption. Moreover, as pointed out in § 5.1, the use of abundances derived from beam-averaged column densities could be underestimates if the source size is significantly smaller than the beam. In our case this is likely for the molecules showing high rotational temperatures (e.g. HNCO, CH_2CO, NH_2CN, NH_2CHO, CH_3OCHO, CH_3OCH_3, and C_2H_5CN).

In general, the chemical composition of Sgr B2 seems to be a mixture of the chemistry of the Hot Core (HC) and the Compact Ridge (CR) sources in Orion. The oxygen-bearing species characteristic for the CR, e.g. H_2CO, CH_3OH, CH_3OCHO, and CH_3OCH_3, are all detected in Sgr B2 but have somewhat lower abundances. Also the nitriles typical for the HC, e.g. CH_3CN, C_2H_3CN, and C_2H_5CN, are readily detected in the cores of Sgr B2. Whereas the abundances of CH_3CN and C_2H_3CN are somewhat higher in Sgr B2 as compared to the Orion HC, the more saturated species C_2H_5CN has a similar abundance to that in the HC in Sgr B2(N) if we correct the C_2H_5CN abundance listed in Table 3 for a source size similar to that obtained for CH_3CN (see Table 1). In Sgr B2(M) the C_2H_5CN abundance is somewhat lower than in the HC.

From what was found in the previous section there is a tendency in that the Sgr B2(N) core, somewhat richer in nitriles than M, seems to exhibit more of a HC-type chemistry than CR-type chemistry. On the other hand, the chemical composition in the Sgr B2(M) core seems to reflect HC-type as well as CR-type chemistry at an equal level. Finally, we note the great similarity between the very high SO and SO_2 abundances in the Orion outflow and in Sgr B2(M), indicating prominent outflow chemistry in the latter source as well. It is clear that the concentrations of SO and SO_2 in M are increased by a factor 10^2 and 10^3, respectively, as compared to their abundances in the ambient cloud position NW.

The authors would like to thank the referee and John Black for comments and suggestions that improved and clarified the manuscript. A. N., Å. H., and P. B. acknowledge financial support from The Swedish Natural Science Research Council (NFR). A. N. also gratefully acknowledges support from the New York Center for Studies of the Origins of Life (NSCORT) at RPI under NASA grant NAG 5-7598. W. M. I. was supported by NASA grant NAG 5-8718.

REFERENCES

Blake, G. A., Sutton, E. C., Masson, C. R., & Phillips, T. G. 1987, ApJ, 315, 621
Carlstrom, J. E., & Vogel, S. N. 1989, ApJ, 337, 408
Carroll, T. J., & Goldsmith, P. F. 1981, ApJ, 245, 891
Chin, Y.-N., Henkel, C., Whiteoak, J. B., Langer, N., & Churchwell, E. B. 1996, A&A, 305, 960
Cummins, S. E., Linke, R. A., & Thaddeus, P. 1986, ApJS, 60, 819
De Pree, C. G., Goss, W. M., & Gaume, R. A. 1998, ApJ, 500, 847
de Vicente, P., Martín-Pintado, J., & Wilson, T. L. 1997, A&A, 320, 957
Dickens, J. E., Irvine, W. M., Ohishi, M., Ikeda, M., Ishikawa, S., Nummelin, & A., Hjalmarson, Å. 1997, ApJ, 489, 753
Flower, D. R., Pineau des Forêts, G., & Walmsley, C. M. 1995, A&A, 294, 815
Frerking, M. A., Langer, W. D., & Wilson, R. W. 1982, ApJ, 262, 590
Gardner, F. F., Whiteoak, J. B, Reynolds, J., Peters, W. L., & Kuiper, T. B. H. 1989, MNRAS, 240, 35
Goldsmith, P. F., Irvine, W. M., Hjalmarson, Å., & Ellder, J. 1986, ApJ, 310, 383
Goldsmith, P. F., Krotkov, R., Snell, R. L., Brown, R. D., & Godfrey, P. 1983, ApJ, 274, 184
Goldsmith, P. F., & Langer, W. 1999, ApJ, 517, 209
Goldsmith, P. F., Snell, R. L., Hasegawa, T., & Ukita, N. 1987a, ApJ, 314, 525
Goldsmith, P. F., Snell, R. L., & Lis, D. C. 1987b, ApJ, 313, L5
Goldsmith, P. F., Lis, D. C., Lester, D. F., & Harvey, P. M. 1992, ApJ, 389, 338
Gordon, M. A., Berkermann, U., Mezger, P. G., Zylka, R., Haslam, C. G. T., Kreysa, E., Sievers, A., & Lemke, R. 1993, A&A, 280, 208
Greaves, J. S., & Nyman, L.-Å. 1996, A&A, 305, 950
Henkel, C., Wilson, T. L., Walmsley, C. M., & Pauls, T. 1983, A&A, 127, 388
Hüttemeister, S., Wilson, T. L., Henkel, C., & Mauersberger, R. 1993, A&A, 276, 445
Hüttemeister, S., Wilson, T. L., Mauersberger, R., Lemme, C., Dahmen, G., & Henkel, C. 1995, A&A, 294, 667
Irvine, W. M., Goldsmith, P. F., & Hjalmarson, Å. 1987, in Interstellar Processes, ed. D. J. Hollenbach & H. A. Thronson (Dordrecht: Reidel), 561
Irvine, W. M. I., Schloerb, F. P., Hjalmarson, Å., & Herbst, E. 1985, in Protostars & Planets II, ed. D. C. Black & M. S. Matthews (Tucson: Univ. Arizona Press), 579
Johnson, D. R., Lovas, F. J., & Kirchhoff, W. H. 1972, J. Phys. Chem. Ref. Data, 1, 1011
Kaifu, N., Morimoto, M., Nagane, K., Akabane, K., Iguchi, T., & Takagi, K. 1974, ApJ, 191, L135
Kuan, Y.-J., Mehringer, D. M., & Snyder, L. E. 1996, ApJ, 459, 619
Lampton, M., Margon, B., & Bowyer, S. 1976, ApJ, 208, 177
Lis, D. C., & Goldsmith, P. F. 1989, ApJ, 337, 704
———. 1990, ApJ, 356, 195
———. 1991, ApJ, 369, 157
Lis, D. C., Goldsmith, P. F., Carlstrom, J. E., & Scoville, N. Z. 1993, ApJ, 402, 238
Lovas, F. J., Suenram, R. D., Snyder, L. E., Hollis, J. M., & Lees, R. M. 1982, ApJ, 253, 149
Martín-Pintado, J., de Vicente, P., Wilson, T. L., & Johnston, K. J. 1990, A&A, 236, 193
Miao, Y., & Snyder, L. E. 1997, ApJ, 480, L67
Nummelin, A., & Bergman, P. 1999, A&A, 341, L59
Nummelin, A., Bergman, P., Hjalmarson, Å., Friberg, P., Irvine, W. M., Millar, T. J., Ohishi, M., & Saito, S. 1998a, ApJS, 117, 427 (Paper I)
Nummelin, A., Dickens, J. E., Bergman, P., Hjalmarson, Å., Irvine, W. M., Ikeda, M., & Ohishi, M. 1998b, A&A, 337, 275
Ohishi, M. 1992, in Chemistry and Spectroscopy of Interstellar Molecules, ed. D. K. Bohme et al. (Tokyo: Univ. Tokyo Press), 23
Pearson, J. C., Sastry, K. V. L. N., Herbst, E., & De Lucia, F. C. 1997, ApJ, 480, 420
Penzias, A. A. 1981, ApJ, 249, 518
Plummer, G. M., Herbst, E., & De Lucia, F. C. 1987, ApJ, 318, 873
Prantzos, N., Aubert, O., & Audouze, J. 1996, A&A, 309, 760
Scoville, N. Z., Solomon, P. M., & Penzias, A. A. 1975, ApJ, 201, 352
Schilke, P., Walmsley, C. M., Pineau des Forêts, G., Roueff, E., Flower, D. R., & Guilloteau, S. 1992, A&A, 256, 595
Sutton, E. C., Jaminet, P. A., Danchi, W. C., & Blake, G. A. 1991, ApJS, 77, 255
Turner, B. E. 1989, ApJS, 70, 539
———. 1991, ApJS, 76, 617
Vogel, S. N., Genzel, R., & Palmer, P. 1987, ApJ, 316, 243
van Dishoeck, E. F., & Blake, G. A. 1998, ARA&A, 36, 317
Whiteoak, D. R., & Gardner, F. F. 1981, MNRAS, 197, 39
Wilson, T. L., & Rood, R. T. 1994, ARA&A, 32, 191
Wyrowski, F., Schilke, P., & Walmsley, C. M. 1999, A&A, 341, 882
Xie, T., Goldsmith, P. F., Snell, R. L., & Zhou, W. 1993, ApJ, 402, 216
Ziurys, L. M., Apponi, A. J., Hollis, J. M., & Snyder, L. E. 1994, ApJ, 436, L181
Zmuidzinas, J., Blake, G. A., Carlstrom, J., Keene, J., & Miller, D. 1995, ApJ, 447, L125

THE ASTROPHYSICAL JOURNAL SUPPLEMENT SERIES, 132:127, 2001 January

ERRATUM

In the paper "A Three-Position Spectral Line Survey of Sagittarius B2 between 218 and 263 GHz. II. Data Analysis" by A. Nummelin, P. Bergman, Å. Hjalmarson, P. Friberg, W. M. Irvine, T. J. Millar, M. Ohishi, and S. Saito (ApJS, 128, 213 [2000]), the affiliations for M. Ohishi and S. Saito were set incorrectly. The correct affiliation for M. Ohishi is National Astronomical Observatory of Japan, 2-21-1, Osawa, Mitaka, Tokyo 181-8588, Japan; ohishi@nao.ac.jp. The correct affiliation for S. Saito is Research Center for Development of Far-Infrared Region, Fukui University, 3-9-1 Bunkyo, Fukui 901-8507, Japan; saito@maxwell.apphy.fukui-u.ac.jp. The Press sincerely regrets this error.